SWIRE: The *SIRTF* Wide-Area Infrared Extragalactic Survey

Carol J. Lonsdale,[1] Harding E. Smith,[1,2,3] Michael Rowan-Robinson,[4] Jason Surace,[1] David Shupe,[1] Cong Xu,[1]
Sebastian Oliver,[5] Deborah Padgett,[1] Fan Fang,[1] Tim Conrow,[1] Alberto Franceschini,[6] Nick Gautier,[7] Matt Griffin,[8]
Perry Hacking,[9] Frank Masci,[1] Glenn Morrison,[1] Joanne O'Linger,[1] Frazer Owen,[10] Ismael Pérez-Fournon,[11]
Marguerite Pierre,[12] Rick Puetter,[2,13] Gordon Stacey,[14] Sandra Castro,[1] Maria Del Carmen Polletta,[1]
Duncan Farrah,[1] Tom Jarrett,[1] Dave Frayer,[1] Brian Siana,[2,3] Tom Babbedge,[4] Simon Dye,[4] Matt Fox,[4]
Eduardo Gonzalez-Solares,[5] Malcolm Salaman,[5] Stefano Berta,[6] Jim J. Condon,[15] Hervé Dole,[16]
and Steve Serjeant[17]

ABSTRACT. The *SIRTF* Wide-Area Infrared Extragalactic Survey (SWIRE), the largest *SIRTF* Legacy program, is a wide-area imaging survey to trace the evolution of dusty, star-forming galaxies, evolved stellar populations, and active galactic nuclei (AGNs) as a function of environment, from redshifts $z \sim 3$ to the current epoch. SWIRE will survey seven high-latitude fields, totaling 60–65 deg^2 in all seven *SIRTF* bands: Infrared Array Camera (IRAC) 3.6, 4.5, 5.6, and 8 μm and Multiband Imaging Photometer for *SIRTF* (MIPS) 24, 70, and 160 μm. Extensive modeling suggests that the Legacy Extragalactic Catalog may contain in excess of 2 million IR-selected galaxies, dominated by (1) ~150,000 luminous infrared galaxies (LIRGs; $L_{\mathrm{FIR}} > 10^{11}\ L_{\odot}$) detected by MIPS (and significantly more detected by IRAC), ~7000 of these with $z > 2$; (2) 1 million IRAC-detected early-type galaxies (~2×10^5 with $z > 1$ and ~10,000 with $z > 2$); and (3) ~20,000 classical AGNs detected with MIPS, plus significantly more dust-obscured quasi-stellar objects/AGNs among the LIRGs. SWIRE will provide an unprecedented view of the evolution of galaxies, structure, and AGNs.

The key scientific goals of SWIRE are (1) to determine the evolution of actively star forming and passively evolving galaxies in order to understand the history of galaxy formation in the context of cosmic structure formation; (2) to determine the evolution of the spatial distribution and clustering of evolved galaxies, starbursts, and AGNs in the key redshift range $0.5 < z < 3$ over which much of cosmic evolution has occurred; and (3) to determine the evolutionary relationship between "normal galaxies" and AGNs and the contribution of AGN accretion energy versus stellar nucleosynthesis to the cosmic backgrounds. The large area of SWIRE is important to establish statistically significant population samples over enough volume cells that we can resolve the star formation history as a function of epoch and environment, i.e., in the context of structure formation. The large volume is also optimized for finding rare objects.

The SWIRE fields are likely to become the next generation of *large* "cosmic windows" into the extragalactic sky. They have been uniquely selected to minimize Galactic cirrus emission over large scales. The *Galaxy Evolution Explorer* will observe them as part of its deep 100 deg^2 survey, as will *Herschel*. SWIRE includes ~9 deg^2 of the unique large-area *XMM* Large Scale Structure hard X-ray imaging survey and is partly covered by the UKIDSS deep *J* and *K* survey. An extensive optical/near-IR imaging program is underway from the ground.

The SWIRE data are nonproprietary; catalogs and images will be released twice yearly, beginning about 11 months after *SIRTF* launch. Details of the data products and release schedule are presented.

[1] Infrared Processing and Analysis Center, California Institute of Technology, 100-22, Pasadena, CA 91125; cjl@ipac.caltech.edu.

[2] Center for Astrophysics and Space Sciences, University of California, San Diego, La Jolla, CA 92093-0424; hsmith@ucsd.edu.

[3] Also Department of Physics, University of California, San Diego.

[4] Astrophysics Group, Blackett Laboratory, Imperial College, Prince Consort Road, London SW7 2BW, UK.

[5] Astronomy Centre, CPES, University of Sussex, Falmer, Brighton BN1 9QJ, UK.

[6] Dipartimento di Astronomia, Università di Padova, Vicolo Osservatorio 5, I-35122 Padua, Italy.

[7] Jet Propulsion Laboratory, 264-767, 4800 Oak Grove Drive, Pasadena, CA 91109.

[8] Department of Physics and Astronomy, University of Wales, Cardiff, 5 The Parade, Cardiff CF24 3YB, UK.

[9] Department of Astronomy, El Camino College, 16007 Crenshaw Boulevard, Torrance, CA 90506.

[10] National Radio Astronomy Observatory, P.O. Box O, Socorro, NM 87801.

[11] Instituto de Astrofísica de Canarias, 38200 La Laguna, Tenerife, Spain.

[12] CEA/DSM/DAPNIA, Service d'Astrophysique, 91191 Gif-sur-Yvette, France.

[13] Pixon LLC, 9295 Farnham Street, San Diego, CA 92123.

[14] Department of Astronomy, Cornell University, 220 Space Science Building, Ithaca, NY 14853.

[15] National Radio Astronomy Observatory, 520 Edgemont Road, Charlottesville, VA 22903.

[16] Steward Observatory, University of Arizona, 933 North Cherry Avenue, Tucson, AZ 85721.

[17] Centre for Astronomy and Planetary Science, School of Physical Sciences, University of Kent at Canterbury, Canterbury, Kent CT2 7NZ, UK.

1. SCIENTIFIC GOALS OF SWIRE

1.1. Modes and Rates of Star Formation

With the *SIRTF* Wide-Area Infrared Extragalactic Survey (SWIRE), we seek to directly measure the light of both dusty galaxies and evolved stellar populations at $z < 3$ (universe age greater than 2 Gyr),[18] with enough galaxy and volume cell statistics to fully sample the range of density environments from dense clusters to voids.

From a theoretical viewpoint, the standard cosmological paradigm—that we live in a ΛCDM universe that began with the big bang followed by an inflationary period—has been exceedingly successfully in explaining the major cosmological observations, including the cosmic microwave background (CMB) and its spatial structure, the power spectrum of the CMB, cosmic nucleosynthesis, the large-scale filamentary structure of the cosmic web of galaxies, and dark matter halos.

When it comes to galaxy formation and evolution, the observational situation becomes much more complex because we most easily study light, whereas theory directly predicts only the distribution and merging history of the underlying mass distribution, and the relation between the two depends on complex, usually nonlinear, astrophysical processes. In spite of this, hierarchical theories have also been remarkably successful at predicting the overall scheme of galaxy formation and evolution: that it is dominated by merging of clumps within dark matter halos and the steady accretion of gas into disks, that it was at peak activity at $z \sim 1$–3, that it seems to have occurred faster in higher density environments, and that it has declined sharply since $z \sim 1$. The morphology of galaxies seems to have evolved strongly, driven by both major and minor mergers and by episodes of gas accretion, and the Hubble sequence as we now know it seems to have come into being between redshifts 1 and 2.

Mid- and far-infrared observations of evolving galaxies are essential because a large fraction of emitted starlight in galaxies is absorbed and reemitted by dust in the thermal infrared. The *COBE* detection of the cosmic infrared background (CIB) has illustrated that more than 50% of the total luminous energy density of the universe emerges longward of ~ 1 μm (Hauser & Dwek 2001). An even higher fraction of a galaxy's light (90% or more) can emerge in the far-infrared in starbursts, which may be a significant mode of star formation over the history of the universe. The most extreme IR objects are the ultraluminous IR galaxies (ULIRGs), with quasi-stellar object (QSO)–scale luminosities ($>10^{12} L_\odot$), which are very rare in the local universe.

The *Infrared Space Observatory* (*ISO*) satellite made several important surveys at 6.7, 15, 90, and 170 μm, resulting in star formation histories that increase even more steeply back in time

than observed in the UV-optical (Rowan-Robinson et al. 1997; Elbaz et al. 1999). Perhaps most surprisingly, a large population of faint submillimeter sources has been discovered, using the Submillimeter Common-User Bolometric Array (SCUBA) on the James Clerk Maxwell Telescope, which represent a population of very luminous objects at redshifts $z = 2$–4 with a much higher space density than the local ULIRGs (Blain et al. 2002; Chapman et al. 2003). These populations and the integrated CIB have been modeled successfully using phenomenological models (Rowan-Robinson 2001; Chary & Elbaz 2001; Xu et al. 2001), some of which require high rates of luminosity evolution, $L \propto (1 + z)^4$. Moreover, the star formation efficiencies of the high-z ULIRGs may have been much higher than now; Blain et al. (1999) find the halo mass–to–infrared light ratio of a typical merger at $z = 3$ to be ~ 200 times smaller than today.

These results challenge hierarchical models conceptually because it is expected that galaxy masses grow slowly as smaller systems merge and gas accretes. Indeed, no CDM-based model, whether semianalytic or *N*-body, has successfully reproduced the observed numbers of high-redshift ULIRGs from the submillimeter data (Guiderdoni et al. 1998; Fardal et al. 2001; Devriendt & Guiderdoni 2000; Somerville et al. 2001; R. S. Somerville 2003, private communication). Instead, very high star formation rates (SFRs) at early times are more reminiscent of monolithic collapse theories than the standard hierarchical theory. In an extreme case, too much star formation in bursts at high redshift will conflict with the conversion rate of baryonic matter into stars that is derived from deep *K*-band studies (Dickinson et al. 2003).

There are significant unknowns associated with these studies of the evolving IR galaxy populations. A major one is the dust temperature: with only a single 850 μm detection on the Rayleigh-Jeans tail of the Planck spectrum, the temperature is unconstrained and the luminosity and SFR can be uncertain by up to 2 orders of magnitude (Kaviani, Haehnelt, & Kauffmann 2003). Rowan-Robinson (2001) suggests that the high-redshift IR population might be dominated by cooler dust emission from larger disks than the sub-kiloparsec–scale warm dust sources that seem to characterize local ULIRGs, and indeed Chapman et al. (2002) find evidence for some cool *ISO* sources at $z \sim 1$. Other unknowns include the timescale for starbursts at high redshift, the form of the initial mass function (IMF) in starbursts (an IMF truncated at the low-mass end would reduce conflicts between the observed luminosities and the conversion rate of gas to stars; Franceschini et al. 2001), and the contribution to the IR luminosities of dust-enshrouded active galactic nuclei (AGNs).

SWIRE is designed to provide unique and essential information about star formation rates and modes between about $0.5 < z < 3$. The multiple bands spanning the thermal infrared from 4 to 160 μm provide unprecedented coverage of the spectral energy distribution (SED), which will allow an accurate estimate of the luminosity of the warmer dust components out

---

[18] $H_0 = 75$ km s^{-1} Mpc^{-1}, $\Omega_\Lambda = 0.7$, $\Omega_m = 0.3$, which we adopt throughout except for some length scales and volumes quoted in $H_0 = 100\, h$ km s^{-1} Mpc^{-1} units.

to redshifts ∼2 and cooler components to lower redshifts. Color-dependent luminosity functions will elucidate starburst versus quiescent star formation rates and starburst timescales versus AGN processes. SWIRE will address how star formation in IR-luminous systems differed at early times from today. The majority of SWIRE dusty populations will be LIRGS ($L \sim 10^{11} L_\odot$) at $z \sim 1$, when bulges and disks were fully coming into being, so we can study star formation rates associated with these processes directly. The $z > 2$ SCUBA sources had much higher star formation efficiency than local ULIRGs; did they simply have more prodigious nuclear starbursts (local ULIRGs concentrate their starbursts within the central 1 kpc and frequently the central 100 pc)? Or did they sport extensive disks with high star formation efficiencies throughout, driven by high rates of gas accretion in galaxy clusters? Or are they enormous mergers with extensive regions of distributed star formation? The dust temperature associated with these episodes will be a strong discriminator because higher-density star-forming regions typically reach higher dust temperatures.

The large SWIRE fields will allow us to track these processes as a function of environment in hundreds of volume cells from rich clusters to the "field." For example, we can search for the CDM-predicted trend for active star formation to be more closely confined to the denser regions of the universe at the higher redshifts, and as star formation rates decrease in overall strength with cosmic time, to move systematically to less and less dense environments.

The large volume of SWIRE is also uniquely important for the discovery of rare objects; a large "shallow" extragalactic survey can cover more volume than the same amount of time spent on a smaller, deeper one (Condon et al. 1998), as demonstrated by the success of the Sloan Digital Sky Survey at finding $z > 5$ QSOs (Fan et al. 2003). In particular, SWIRE has much more volume sensitivity to $z \sim 3$ ULIRGs than current submillimeter surveys, with the potential to detect ∼100 $z > 3$ ULIRGs per square degree by their 8 and/or 24 μm flux, according to the models of Xu et al. (2003), which are consistent with faint submillimeter counts and redshift distributions and the CIB. Thus, SWIRE will confirm the presence of a substantial population of high-z ULIRGs, improve estimates of their luminosities and SFRs, and trace their clustering properties. Intriguingly, there is tentative evidence to suggest that high-z submillimeter sources may be clustered (Scott et al. 2002; Almaini et al. 2003), as might be expected if these events trace the highest density environments at these redshifts. According to semianalytic star-formation scenarios (e.g., Somerville et al. 2001), ULIRGs at high z may be tracers of already formed massive halos. Although at low redshift, ULIRGs are associated with violent mergers and are not found in massive halos (rich clusters), at earlier epochs galaxy building occurred first in the deepest potential wells, and distant ULIRGs may be the progenitors of current cluster spheroids. SWIRE may detect enough ULIRGs at $z > 2.5$ with halos of mass $\geq 10^{13} M_\odot$ to allow a statistical estimate of σ_8, the rms fluctuation of the mass distribution on $8\ h^{-1}$ Mpc scales; the predicted number density of such halos varies by a factor of ∼6 at $z \sim 2.5$ for $0.7 < \sigma_8 < 0.9$ (R. S. Somerville 2003, private communication).

1.2. Spheroids

While dust emission in galaxies tracks the most recently formed stellar populations, the SEDs of passively evolving older stellar populations peak in the near-infrared, and the wavelength bands of *SIRTF*'s Infrared Array Camera (IRAC) were selected (in part) to optimize study of them at high redshifts. A fundamental goal of *SIRTF*/IRAC is to establish the evolution of the mass and luminosity functions of evolved stellar populations and relate them to the morphological and color evolution of galaxies and the establishment of the Hubble sequence (Simpson & Eisenhardt 1999). Is there a significant population of high-redshift evolved systems that formed at very high redshift in a "monolithic collapse" scenario, as perhaps indicated by the SCUBA sources, or can hierarchical models fully explain the formation of massive galaxies and spheroids at moderate redshifts from merging of preexisting galaxian units? Are the stellar populations of distant spheroids being formed in substantial amounts at $1 < z < 2$, or are older stellar populations being dynamically assembled into massive systems at these moderate epochs?

Fossil evidence in the local universe favors a uniform, high-redshift formation epoch for massive cluster ellipticals; in particular, the tightness of the fundamental plane and the enrichment of massive systems with α-elements (Ellis et al. 1997) point to rapid homogeneous star formation episodes at high redshift. However, recent *Hubble Space Telescope* (*HST*) imaging of distant spheroids has revealed substantially more morphological than color evolution at $z < 2$–3, revealing increasing evidence for mergers and peculiarities with increasing redshift (Conselice 2003; Phillips et al. 2001) and evidence for significant color inhomogeneities (Benson et al. 2001; Menanteau et al. 1999; Kajisawa & Yamada 2001). Estimates for the stellar masses and the stellar mass buildup with redshift of a deep K-band sample in the Hubble Deep Field–North (HDF-N; Dickinson et al. 2003) indicate that only 3%–14% of the present-day mass in stars had formed by $z \sim 2.7$ and 50%–75% had formed by $z \sim 1$. This is in agreement with some hierarchical models (between which there is significant dispersion in predictions), but apparently in disagreement with models in which the bulk of stars in present-day spheroids formed at very early times ($z \gg 2$). On the other hand, Benson et al. (2001) find that hierarchical models underpredict the proportion of high-redshift, homogeneous, passively evolving objects, and Labbe et al. (2003) find a much larger population of red systems with $z_{phot} > 2$ in the Hubble Deep Field–South (HDF-S) than Dickinson et al. (2003) do in HDF-N. Conselice (2003) finds that the rate of major mergers among the most massive systems increases strongly with z, reaching ∼50% at $z > 2.5$, in qualitative

agreement with the hierarchical picture. On the other hand, massive systems with rapid star formation must already be in place at $z \sim 3$, an observation that is difficult to reconcile with slow stellar mass buildup predictions of some hierarchical models, such as Cole et al. (2000). Central to these discussions is the cosmological model assumed; e.g., Phillips et al. (2001) find morphological number counts in the HDFs inconsistent with the large Ω_Λ implied by current concordance cosmology.

SWIRE/IRAC will directly provide the accumulated mass in evolved stars measured from the r' to 5 μm SEDs. IRAC design was in part optimized for measuring the stellar mass of distant systems, and the GOODS Legacy program takes this science to the deepest possible *SIRTF* limit in a very small region of sky. Ground-based and *HST* NICMOS studies are limited to $\lambda < 2.5$ μm, corresponding to $z < 0.6$ for the $\sim \lambda_{rest} = 1.6$ μm SED peak of evolved stellar systems. IRAC therefore provides much more robust determination of stellar masses to much higher redshifts (Sawicki 2002; Dickinson et al. 2003[19]; Franceschini et al. 2003). SWIRE/IRAC observations are very well matched in depth to SWIRE dusty galaxy observations, sampling the important $z = 1$–2 redshift range over which low matter density cosmological models predict much evolution.

A key advantage of SWIRE's large-area coverage is that these questions can be addressed using large samples over many contiguous volume cells, thus minimizing cosmic variance problems, such as those implied between HDF-N and HDF-S, as mentioned above. Moreover, we naturally expect a strong dependence of cosmic evolution and the timescales of galaxy formation on the local matter density, so it is important to survey the full matter density range in a homogenous fashion.

1.3. Active Galaxies

The fundamental cosmogonic questions concerning AGNs include (1) the true distribution of physical processes underlying the zoo of observational classes of AGNs, (2) the connections between galaxy formation and black hole growth and activity, (3) the importance of AGN contributions to reionizing the universe, and (4) the contribution of gravitational energy from AGNs to the overall luminous energy density of the universe as a function of redshift.

The most challenging aspect of AGN research over the years has been in assembling complete samples, because AGNs suffer very strong observational selections effects of many kinds, which are very difficult to separate from intrinsic physical differences. SWIRE will be one of the best ever surveys for AGNs because many AGN classes emit strongly in the mid-IR, where extinction is low and where SWIRE has excellent volume sensitivity. In particular, many AGNs have warmer mid- to far-infrared colors than star formation–dominated galaxies and thus will be preferentially selected by the highly sensitive 8 and 24 μm *SIRTF* bands.

---

[19] http://www.stsci.edu/science/goods.

Moreover, evidence is now very strong for the existence of a substantial population of AGNs that are heavily absorbed and are strong mid- to far-IR emitters. Highly reddened and absorbed AGNs are turning up in radio, hard X-ray, and near-infrared surveys (Maiolino et al. 1998; Gregg et al. 2002; Cutri 2001). Some of these populations are consistent with the classical AGN unification picture featuring axisymmetrical distributions of surrounding absorbing material, and others favor a young AGN turning on during a merger/starburst episode, deeply embedded in obscuring material from most or all vantage points. Furthermore, the long-standing puzzle over the mismatch between the spectral slope of the cosmic X-ray background and that of its presumed constituent quasars may be solved now that the X-ray background (XRB) is close to being resolved by *XMM* and *Chandra* and is found to be well explained by a population of high column AGNs that increases in number density with redshift (Comastri et al. 2001; Gilli et al. 2001; Polletta et al. 2003).

A major SWIRE goal is therefore to determine the evolving number density of AGNs, particularly heavily obscured ones, and to quantify much better than any other survey their number density at $z > 1$ and their contribution to the CIB; see Polletta et al. (2003) for a recent model. A difficulty with this goal concerns the most heavily obscured AGNs, which can have columns over $N_H \sim 10^{25}$ cm^{-2} (Maiolino et al. 2000) and which can therefore be optically thick even in the near- and mid-IR and thus not recognizable even in SWIRE mid-IR colors. Thus, it is most important to undertake hard X-ray surveys in SWIRE fields. The *XMM* Large Scale Structure Survey (*XMM*-LSS) field (§ 1.5) will be our prime one for obscured AGN studies.

The other key wavelength range for detection of heavily obscured AGNs is the radio, thus a systematic deep radio survey would be of great value in the SWIRE fields. The remarkably tight FIR/radio correlation for star-forming galaxies can be used as a tool for identifying radio-loud AGNs. Only with radio and hard X-ray surveys can the population of dust-shrouded AGNs be recognized and discriminated from starbursts.

SWIRE can be expected to make direct and unique contributions to the AGN unification debate as a result of the size and completeness of its AGN samples. SWIRE will constrain the IR properties of AGNs of all types over large volumes and all environments; how many of the known AGN classes are IR-loud, and how does IR-loudness relate to other AGN properties and to the presence of a starburst? SWIRE will also track the IR evolution of all IR-loud AGN classes over a substantial redshift range, addressing the global evolutionary connections between them.

Another important SWIRE goal is to understand the "starburst-AGN connection." The locally observed correlation between the masses of black holes and their surrounding stellar bulges (Magorrian et al. 1998) implies that the formation of the two are linked, yet we do not understand how. Clues must come from the relationship between star formation and black

hole accretion in active galaxies, since it is widely believed that merger-driven starbursts are effective bulge builders. A close phenomenological relationship between starbursts and AGNs has been recently suggested by Franceschini et al. (2002) on the basis of deep combined IR and *XMM-Newton* observations. How are starbursts and AGNs triggered in active galaxies? How does AGN feedback affect starburst activity and vice versa?

In the local universe, IR-luminous starburst and AGN activity is often triggered by galaxy mergers, especially for the most luminous ULIRGs ($L_{1-1000} > 10^{12} L_{\odot}$; Surace, Sanders, & Evans 2000; Farrah et al. 2001). At high redshift, however, the trigger for starburst/AGN activity of the luminous submillimeter sources is not known. Possibilities include multiple mergers between many small galaxies or even collapse of a large disk of gas to form a protogalaxy (Farrah et al. 2002b); the latter possibility is hinted at by models for high-z submillimeter sources that suggest a cirrus origin for the submillimeter emission (Efstathiou & Rowan-Robinson 2003).

Once triggered, the effects of starburst and AGN activity on each other are currently the subject of debate. Theoretical arguments (Silk & Rees 1998) suggest that the onset of AGN activity will curtail a starburst because of superwinds from the AGN, and indeed modeling of starburst and AGN activity in protogalaxies (Granato et al. 2001) and of black hole (BH) and spheroid formation (Archibald et al. 2002) suggest that most of the star formation must have taken place before the onset of AGN activity. Conversely, there is substantial observational evidence (Priddey & McMahon 2001; Farrah et al. 2002a) that starburst and AGN activity can be coeval in QSOs and hyperluminous infrared galaxies ($L_{1-1000} > 10^{13} L_{\odot}$); many of these systems contain a luminous AGN together with star formation rates (inferred from submillimeter observations) so high that it is unphysical to argue that they are not at or near their peak.

1.4. Large-Scale Structure

Theories of structure formation were strongly constrained by the statistical measurements of clustering in some of the early galaxy redshift surveys. Surveys of infrared galaxies, in particular, were able to rule out the then-standard cold dark matter (CDM) model (Efstathiou et al. 1990; Saunders et al. 1991). Present-day redshift surveys such as the Two Degree Field Galaxy Redshift Survey (2dFGRS; Colless et al. 2001), the Sloan Digital Sky Survey (SDSS; York et al. 2000), and in the far-infrared, the Point Source Catalog Redshift Survey (PSC-z; Saunders et al. 2000), are now able to provide definitive measurements of the galaxy clustering in the local universe.

Despite this success, we have always known that galaxies are biased tracers of the matter distribution. The evidence for this is that different types of galaxies cluster differently (Babul & Postman 1990; Lahav, Nemiroff, & Piran 1990; Oliver et al. 1996; Norberg et al. 2002). If $\Omega_m \sim 0.3$, then some dynam-

ical comparisons of the galaxy velocity field and density fields are consistent only if bias is included (Dekel 1994; Strauss & Willick 1995; Rowan-Robinson et al. 2000), while other comparisons do not require bias (Willick & Strauss 1998), and recent studies of 2dFGRS redshift-space distortions are also consistent with no bias (Lahav et al. 2002). Bias is expected because galaxies represent only a small fraction of the total mass, and even in very simplistic models where galaxies form at the peak of the mass distribution, this produces a bias (Kaiser 1984). The strong interactions seen in actively star forming ULIRGs also provide circumstantial evidence that galaxy formation depends on the environment in which galaxies find themselves, which would also lead one to expect a bias. Until this question of bias is resolved, the modern galaxy surveys will be unable to probe the clustering properties of the underlying mass field and thus test the cosmological models that relate these to the CMB fluctuations.

Recently, models of structure formation have included physically motivated mechanisms for galaxy formation to predict the spatial and temporal evolution of galaxies, using either semianalytic prescriptions or hydrodynamic N-body simulations (Pearce et al. 2001; Somerville et al. 2001; Benson et al. 2001; Blanton et al. 2000). By predicting the clustering properties (and their evolution) of different types of galaxies, such models provide testable explanations of galaxy bias. However, this field is still in its infancy, partially because of a lack of observational constraints over a significant redshift baseline.

SWIRE is able to make two key contributions to the understanding of bias and constraining structure formation models of galaxy formation: the survey samples very different populations of galaxies within the same volume of the universe, and it provides a good sampling of large volumes at high redshift.

We illustrate the large-scale structure parameter space that SWIRE and other surveys could probe in Figure 1 and Table 1. The parameters of interest are the spatial scale of clustering l and the redshift z. To judge how a survey probes this parameter space, we imagine the survey out to z to be divided into cells with volume l^3 and assume that a cell has to have a mean density above one galaxy per cell to be included, and that 100 cells are required for a useful clustering analysis. We also imposed a minimum redshift below which the mean density of the survey is poorly determined because of sampling variance.

1.5. Clusters and the *XMM*-LSS Field

As outlined above, measuring high-redshift clustering is one of the challenges of modern observational cosmology. Whereas galaxies are often considered as difficult objects to understand in terms of initial density fluctuations, clusters of galaxies, in a first approximation, are simpler and complementary. Indeed, an ab initio theory exists (and is well tested by N-body simulations) to describe how the cluster density variations relate to the dark matter density variation (biasing), while such a relation does not exist for galaxy formation. Moreover, clusters
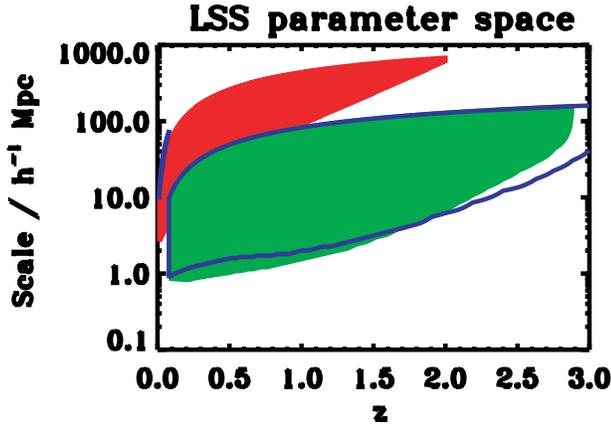
LSS parameter space

Fig. 1.—Large-scale structure parameter space probed by various surveys. We have assumed that to measure clustering statistics, a survey needs at least 100 cells above a threshold mean density of one galaxy per cell. *Solid green and blue outline:* Model spheroids at 3.6 μm and model starbursts at 24 μm from Rowan-Robinson (2001), respectively. For comparison, we show the *IRAS* PSC-z sample (solid blue at low z) from Saunders et al. (2000) and the SDSS early data release spectroscopic sample (*red*) from York et al. (2000), to which we have fitted the following empirical function: $dn/dz = az^2 e^{-(z/0.035)^{1.5}} + bz^2 e^{-(z/0.15)^{1.5}}$, with $a = 1.15 \times 10^8$, $b = 3.1 \times 10^5$. The scale length (*y-axis*) illustrates the size of cells that can be probed. The clustering that can be studied on a particular scale (*x-axis*) is usually constrained by the number of cells criterion at low z and number density threshold at high z.

are the most massive relaxed entities of the universe, located at the intersection of the cosmic filaments; cluster growth occurs by matter accretion flowing along the filaments. Studies of structure evolution and of cluster abundance can independently check cosmological parameter values determined from CMB and supernova studies, as they do not rely on the same physical processes. Last, from the purely physical point of view, clusters represent dense environments, i.e., deep potential wells as well as high concentrations of galaxies, dark matter, and intracluster gas. The entire cluster-group population thus pro-

vides an ideal range of conditions to study environmental effects on the formation of galaxies, active nuclei, and the triggers of star-forming activity.

The number of spectroscopically confirmed clusters beyond $z \sim 0.7$ is still quite small; the reason is simple: detection of high-redshift clusters requires finely tuned multicolor techniques in the optical wave band because of the high surface density of faint background galaxies. Proposed techniques, e.g., adaptive matched filters (Kepner et al. 1999), cluster elliptical red sequence (M. Gladders & H. Yee 2003, in preparation), photometric-redshift classification (Kodama, Bell, & Bower 1999), etc., are very model dependent owing to color evolution of the cluster galaxies, and since they rely primarily on photometric redshifts, they frequently provide large numbers of cluster candidates that are simply portions of cosmic filaments viewed in projection. In parallel, X-ray observations at high Galactic latitude are an important tool for detecting distant clusters because cluster emission, which can be produced only by hot gas trapped in deep potential wells, is extended and easily distinguishable from unresolved QSOs, greatly reducing confusion and projection effects arising in the optical.

In this context, using the unrivaled sensitivity of the *XMM-Newton* Observatory, the *XMM*-LSS has been designed to investigate the large-scale structure of the universe out to a redshift of ~1 as traced by clusters. It will moreover probe the presence of massive clusters out to $z \sim 2$ and enable QSO studies out to $z \sim 4$ with a density of objects some 6 times larger than 2dF. A detailed description of the *XMM*-LSS can be found in Pierre, Valtchanov, & Refregier (2002), and preliminary results can be found in Pierre et al. (2003). The optical counterpart of the X-ray survey is being provided by the CFHT Legacy Survey[20] and is subject to a vigorous spectroscopic follow-up program (Valtchanov et al. 2003; A. G. Willis et al. 2003, in preparation).

---

[20] http://cdsweb.u-strasbg.fr:2001/Science/CFHLS.

TABLE 1
THE POWER OF SWIRE TO PROBE LSS

z	COMOVING LENGTH SCALE (h^{-1} Mpc)					COMOVING VOLUME ($10^9\ h^{-3}$ Mpc^3, 65 deg^2)	MAXIMUM NUMBER OF CELLS		
	6′	30′	1°	2°	4°		10 h^{-1} Mpc^3	50 h^{-1} Mpc^3	100 h^{-1} Mpc^3
(1)	(2)	(3)	(4)	(5)	(6)	(7)	(8)	(9)	(10)
0.1	0.51	2.6	5.1	10	21	0.16	168	1.34	0.16
0.5	2.3	11	23	46	93	15	1.54E+4	123	15
1.0	4.0	20	40	81	162	82	8.21E+4	657	82
1.5	5.3	27	53	107	213	188	1.88E+5	1.6E+3	188
2.0	6.3	32	63	127	253	315	3.15E+5	2.5E+3	315
3.0	7.8	39	78	155	311	581	5.81E+5	4.7E+3	581

NOTE.—This table gives the comoving length scales for given angular separations at different redshifts (cols. [2]–[6]). The smallest SWIRE field has an angular scale of ~2°, and the largest has ~4°. The total volume of the SWIRE survey at different z is provided in col. (7), and the number cells of a given size that the survey can be divided into is in cols. (8)–(10). We have assumed $H_0 = 100\ h^{-1}$ km s^{-1} Mpc^{-1}, $\Omega_m = 0.3$, $\Omega_\Lambda = 0.7$.

TABLE 2
THE SWIRE FIELDS

FIELD	CENTER (J2000.0)		AREA (deg^2)		PRIMARY WINDOW[a]		P.A. (deg east of north)	BACKGROUND $I(100\ \mu m)$ (MJy sr^{-1})
	R.A.	Decl.	MIPS	IRAC	Start	End		
ELAIS S1	00 38 30	−44 00 00	14.32	14.26	Oct 28	Dec 25	293–249	0.42
XMM-LSS	02 21 00	−04 30 00	9.00	8.70	Dec 25	Feb 5	328–343	1.3
CDF-S	03 32 00	−28 16 00	7.14	6.58	Dec 20	Feb 19	303–351	0.46
Lockman	10 45 00	+58 00 00	14.32	14.26	Oct 26	Dec 25	224–179	0.38
Lonsdale	14 41 00	+59 25 00	6.70	6.69	Nov 19	Jul 15	259–28	0.47
ELAIS N1	16 11 00	+55 00 00	9.00	8.70	Dec 16	Sep 3	255–1	0.44
ELAIS N2	16 36 48	+41 01 45	4.45	4.01	Jan 29	Sep 16	216–357	0.42

NOTE.—Units of right ascension are hours, minutes, and seconds, and units of declination are degrees, arcminutes, and arcseconds.

[a] Assuming 2003 August launch. In the event that fields cannot be scheduled in the primary window, secondary windows are as follows: ELAIS S1: May 27–July 26, P.A. = 136°–179°; CDF-S: July 23–September 26, P.A. = 150°–198°; Lockman: March 24–May 23, P.A. = 70°–24°.

The *XMM*-LSS depth ($z_{max} \sim 1$–2 for clusters, $z \sim 4$ for QSOs) matches that of SWIRE very well. Consequently, the combination of the *XMM*-LSS and SWIRE data set over an area of ~9 deg^2 will provide the first coherent study of biasing mechanisms as a function of scale for X-ray–hot (*XMM*), dark (weak lensing), luminous galaxies (optical, SWIRE) and obscured (SWIRE) material as well as unique new insights into the physics of heavily obscured objects.

1.6. Other Fields of Study with SWIRE

Beside the extragalactic topics described above, which drove the design of the SWIRE survey, there are many other studies possible with SWIRE data. These include nearby resolved galaxies, brown dwarfs, evolved stars, circumstellar disks, cirrus emission, and asteroids. While we cannot address all of those topics here, we give a few highlights with further details in § 6.

There are 4542 Two Micron All-Sky Survey (2MASS) galaxies with diameter greater than 5″ in the 2MASS Extended Source Catalog within the SWIRE fields, about 500 of which have diameters greater than 20″. Many of these NIR-selected galaxies may be detected as extended by IRAC.

SWIRE will be exceptionally powerful for brown dwarf detection because of its wide area coverage and sensitivity, potentially able to detect a 5 Gyr old, 275 K brown dwarf at 10 pc. We give estimates of detection statistics in § 6.9.

SWIRE can also provide samples of new debris disks around young stars, unbiased by age or spectral type. We may expect to detect up to 150 of them with the Multiband Imaging Photometer for *SIRTF* (MIPS).

2. THE SWIRE SURVEY

The SWIRE fields are listed in Table 2. The SWIRE survey was designed to take maximum advantage of the unique capabilities of *SIRTF* to further the study of cosmology and of galaxy formation and evolution; it is the widest survey that can be made with the *SIRTF* time available that is commensurate

with robust data quality. In addition, since it is a Legacy survey, an overriding principle in the design of SWIRE was to ensure that the data products would be of long-lasting value for an extremely broad range of scientific investigations, and not just for the few that the SWIRE team itself would be able to undertake.

The depth, area coverage, and number of fields of the SWIRE survey were the result of a trade-off analysis between redshift depth, maximum volume cell size, number of volume cells, number of lines of sight required to minimize cosmic variance, acceptable foreground cirrus noise levels, and total integration time. An initial consideration was that SWIRE complement the already planned deep survey of the Guaranteed Time Observers (GTOs; Fazio et al. 2003[21]; Rieke et al. 2003[22]), which covers 6×0.4 deg^2 to 5 σ photometric sensitivities, ~2 μJy at 3.6 μm and 0.11 mJy at 24 μm.

A governing factor in the SWIRE design was the availability of *SIRTF* astronomical observing templates (AOTs). For MIPS, a natural mode and survey depth for a large-area survey that nicely complements the GTO deep survey is moderate scan speed with two passes of 4 s integrations each (see § 2.2.2 for details). This results in 80 s of integration per point on the sky with a sensitivity at which many models predict the extragalactic sky to be mildly confusion limited to the *SIRTF* 70 μm beam (see Table 3). This then became the depth yardstick for SWIRE.

The total area coverage was selected such that the survey would probe several hundred volume cells of scale ~100 Mpc, enough to sample many different environments within the cosmic web. The number of lines of sight was a trade-off between cosmic variance considerations (more fields) and maximizing the physical size scale probed in each field (fewer, larger fields), moderated by the availability of large sky areas with acceptable

---

[21] http://sirtf.caltech.edu/SSC/geninfo/gto/abs/pid8.

[22] http://sirtf.caltech.edu/SSC/geninfo/gto/abs/pid81.

TABLE 3
PREDICTED SWIRE PHOTOMETRIC SENSITIVITY, CIRRUS, AND CONFUSION NOISE LEVELS

PARAMETER	PHOTOMETRIC SENSITIVITY/NOISE LEVELS						
	μJy	μJy	μJy	μJy	μJy	mJy	mJy
IRAC wavelength (μm)	3.6	4.5	5.8	8.0			
MIPS wavelength (μm)					24	70	160
Sensitivity 5 σ	7.3	9.7	27.5	32.5	450	2.75	17.5
Cirrus noise 5 σ:							
$I_{100} = 0.5$ MJy sr^{-1} (*IRAS*)	2.8E−05	5.4E−05	1.3E−04	7.4E−04	0.31	0.11	11
$I_{100} = 1.0$ MJy sr^{-1}	7.8E−05	1.5E−04	3.6E−04	2.1E−03	0.88	0.32	30
$I_{100} = 2.0$ MJy sr^{-1}	2.2E−04	4.3E−04	1.0E−03	5.9E−03	2.5	0.90	84
Assumed SED	1.3	2.0	3.4	6.4	58	0.49	2.6
Confusion limits:[a]							
Beam FWHM (arcsec)	2.05	2.05	2.08	2.50	5.6	16.7	35.2
Ω_b (10^{-6} deg^2)	0.37	0.37	0.38	0.55	2.74	24.3	108
Xu et al. 2003 model S3+E2	6.2	6.2	5.4	6.7	175	10.0	71
Rowan-Robinson 2001	1.6	1.3	1.1	4.0	190	6.3	60
Rodighiero et al. 2003; Franceschini et al. 2001	5.0	5.0	4.8	4.3	180	6.0	45
Lagache, Dole, & Puget 2003; Dole et al. 2003	...	...	...	4.0	125	6.5	56

[a] Using a source density criterion of 40 beams per source. The beam is assumed to be Gaussian with the quoted FWHM values, which were derived from the prelaunch *SIRTF* beam profiles convolved with the band-dependent pixel sizes (MIPS: Dole et al. 2003; IRAC: this work).

cirrus noise levels. The resulting seven fields project between ~130 and 250 100 h^{-1} comoving Mpc at $z = 2$, with about 50 100 Mpc scale comoving radial distance cells along each line of sight to that epoch.

The SWIRE fields and *SIRTF* prime observation windows are detailed in Table 2, with secondary windows listed for three fields. The expected SWIRE 5 σ photometric sensitivities compared to anticipated cirrus noise (see below) and confusion limits are shown in Table 3. Regarding confusion noise, care must be taken in comparing different predictions, which depend on the underlying source count model, the method used to derive the confusion noise, and the accuracy with which the point-spread function (PSF), the instrument, and the data-taking methods are modeled. A detailed treatment for MIPS is given by Dole, Lagache, & Puget (2003), and predictions based specifically on the SWIRE models, data observation strategy, and data-processing methods are presented by M. Rowan-Robinson et al. (2003, in preparation).

2.1. Field Selection

We considered a number of factors in choosing our survey fields: cirrus contamination, existing or future multiwavelength coverage, observability constraints, and avoidance constraints. A detailed discussion of these will appear in a future paper (S. Oliver et al. 2003, in preparation). Here we discuss each constraint briefly.

Clouds within our own galaxy produces structured infrared emission, "cirrus," which can be confused with extragalactic sources and which causes extinction in the soft X-ray and UV bands. To estimate the level of this cirrus noise, we start from a scaling relationship derived by Helou & Beichman (1990), derived in turn from the power spectrum analysis of cirrus

clouds performed by Gautier et al. (1992):

$$\frac{\sigma_{cir}}{1 \text{ mJy}} \approx 0.3 \left(\frac{\lambda}{100 \text{ } \mu m}\right)^{2.5} \left(\frac{D}{m}\right)^{-2.5} \left[\frac{B(\lambda)}{1 \text{ MJy sr}^{-1}}\right]^{1.5} \quad (1)$$

(we modify this slightly by replacing λ with the larger of λ and 5.8 μm). We have calculated the 5 σ cirrus noise for regions of 0.5, 1, and 2 MJy sr^{-1} and compare these to our intended survey depth (Table 3). The cirrus noise is clearly not important for $\lambda < 24$ μm, but if I_{100} is above 2 MJy sr^{-1}, the cirrus noise exceeds our depth at 160 μm.

When choosing our survey fields, we thus did not consider any field with a cirrus intensity much above 1 MJy sr^{-1}. Since the structure of the cirrus is non-Gaussian and the source confusion limit is highly uncertain, we adopted a more conservative limit of 0.5 MJy sr^{-1} for most of our fields. We performed an exhaustive search over the whole sky considering all fields that met this latter criteria. The cirrus map for one of the fields that we finally selected is contrasted with one that we did not in Figure 2.

As a legacy project, we felt that it was important to select fields that already had a wealth of data. We assembled an extensive list of fields that have been extensively surveyed at a variety of wavelengths (Williams et al. 1996; Oliver et al. 2000). We examined the cirrus in all of these fields and rejected many where the cirrus was too high or where there were only small patches of low cirrus. One field, the *XMM*-LSS field, exceeded our cirrus threshold, but the wealth of survey data over a large area (in particular the *XMM* data) that this field provided was felt to outweigh the risk of compromising the longer wavelength data. We found it necessary to include only
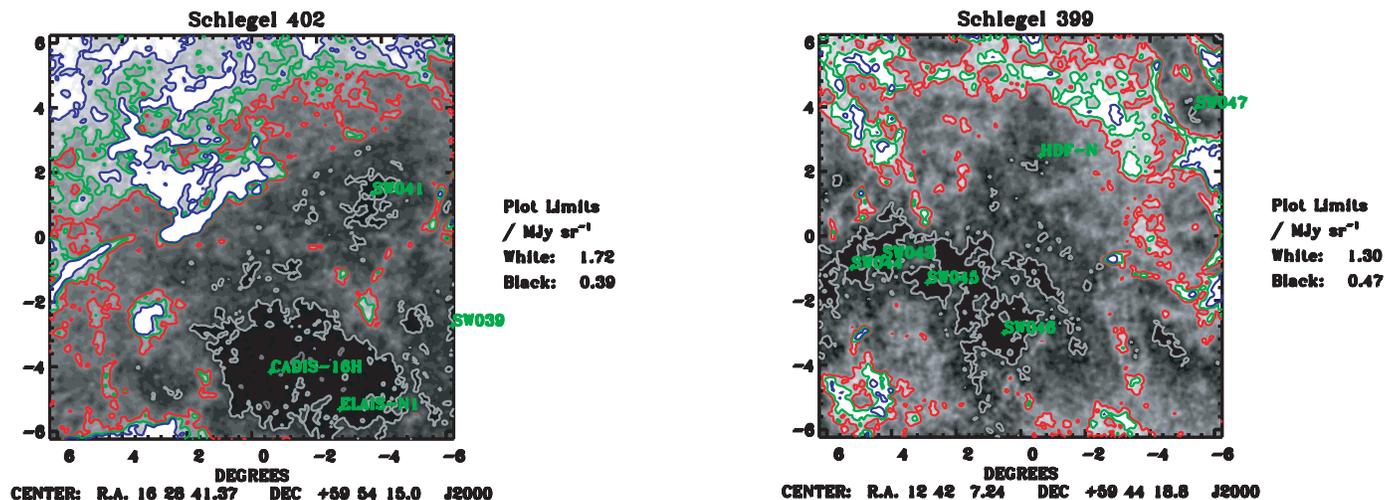
FIG. 2.—Emission from Galactic cirrus. The *IRAS* 100 μm intensity map for our SWIRE field ELAIS N1 (*left panel*) and for a field we rejected, the Hubble Deep Field (*right panel*). Previously identified survey fields are marked, as are new field centers considered in our selection process (marked "SW"). Contours are at 0.5, 1, 1.2, and 1.5 MJy sr^{-1}. Note that the HDF itself is located in a region of relatively high $I(100 \mu m)$ ($\sim$0.7 MJy sr^{-1}) and that "holes" ($<$0.5 MJy sr^{-1}) on the same map are smaller than the ELAIS "hole." The map boundaries are ISSA plates 402 and 399, respectively; the map intensity comes from *IRAS* data that have been normalized to *COBE* (Schlegel, Finkbeiner, & Davis 1998).

one field that did not have extensive multiwavelength data; this was a former WIRE field (Lonsdale).

We also considered the visibility to *SIRTF* (and many other space missions) and thus excluded any fields below an ecliptic latitude of 30°, with the exception of *XMM*-LSS.

To aid ground-based follow-up, we included a similar number of fields in the northern and southern hemispheres and one equatorial field (*XMM*-LSS).

Images of all our fields are available on the SWIRE Web site,[23] and Table 4 details previously observed smaller fields that lie within the large SWIRE areas (excluding extensive ground-based optical and NIR imaging, which is too complex to detail here).

2.2. *SIRTF* Observations

The *SIRTF* observations of the SWIRE fields are designed to return data with high sensitivity and a reasonable number of samples while still covering large areas with both IRAC and MIPS. Since the longest *SIRTF* astronomical observing requests (AORs) are limited to a few hours in duration, our observing strategy requires stitching together dozens of AORs to map each field. Visualizations of IRAC and MIPS AORs for the SWIRE European Large Area *ISO* Survey (ELAIS) S1 field are shown in Figure 3.

2.2.1. IRAC

Our IRAC mapping strategy will result in four 30 s exposures nominally covering each point. We chose the 30 s frame time

as the best trade between sensitivity at the shorter wavelengths and obtaining enough overlapping images for reliable data—particularly because shorter IRAC exposures in the SWIRE regions are expected to be limited by read noise. The four exposures per point are divided between two coverages separated in time to allow discrimination against moving or transient objects.

Each coverage is made from several overlapping AORs. Each IRAC AOR will cover around a square degree. Within each AOR, the map grid spacing is 280″, and two images are taken at each grid point. These exposures are offset slightly using the small-scale cycling dither in the astronomical observing template (AOT). The AORs in each coverage overlap nominally by 120″ when rotation is neglected.

The two coverages are spatially offset by 150″ along both map grid axes to place the center of the grids of one coverage near the interstices of the other coverage grid.

Table 5 lists the sizes of each AOR, in terms of both grid cells and degrees, and the layout of these AORs into the IRAC map. The lower coverage fringes have not been included in the angular extents.

2.2.2. MIPS

Using the MIPS Scan Map AOT with the medium scanning rate, each scan leg of each AOR at 70 and 24 μm will yield 10 overlapping 4 s exposures at each point. The scan legs are spaced by 276″ for an overlap of about 40″ (four 70 μm pixels) between scan legs.

Each sky position is covered by two AORs, separated by hours as for IRAC to allow detection of moving or transient

TABLE 4
SMALLER IMAGING SURVEYS WITHIN THE LARGE SWIRE FIELDS

SWIRE	Survey	Instrument	R.A.	Decl.	Bands	Size (deg²)	Depth[a]
ELAIS S1	ELAIS (1)	*ISO*	00 35	−43 28	7, 15, 90 μm	4	1 mJy[b]
		BeppoSAX/MECS (2)	00 35	−43 28	2–10 keV	1.7	36 ks
	ES1 Radio Survey (3)	ATCA	00 35	−43 28	1.4 GHz	4	80 μJy
XMM-LSS	*XMM*/Moderate Survey (4)	*XMM*	02 24	−05 00	0.5–10 keV	2	20 ks
	Subaru/*XMM-Newton*	*XMM*	02 18	−05 00	0.5–10 keV	1	50, 100 ks
	Deep Survey (5)	Subaru			*R*	1.3	27.5[c]
		SCUBA/SHADES (6)			450, 850 μm	0.25	60, 3 mJy
		VLA			1.4 GHz	~1	60 μJy
	XMM-LSS VLA Survey (7)	VLA	02 24	−04 30	325 MHz	5.6	4 mJy
CDF-S	CDF-S (8, 9)	*Chandra*	03 32	−27 48	0.5–8 keV	0.1	1 Ms
		HST-WFPC (10)			*VI*	17 arcmin²	28.2
		HST-ACS (11)			*BViz*	0.25	*V* ~ 28
		SIRTF/GOODS (11)			3.6–24 μm	160 arcmin²	0.02 mJy[d]
		SIRTF/GTO (12, 13)			3.6–160 μm	0.4	0.11 mJy[e]
Lockman	LH-E	*ROSAT*-HRI (14)	10 53	57 29	0.5–2 keV	0.13	1.2 Ms
		ROSAT-PSPC (14)	10 52	57 21	0.5–2 keV	0.3	200 ks
		XMM (15)	10 53	57 29	0.5–10 keV	0.2	1.1 Ms
		Chandra (16)	10 53	57 29	0.5–8 keV	1.35	5 ks
		ISO (17, 18, 19)	10 52	57 21	7, 15, 90, 175 μm	0.1–0.5	3 mJy[b]
		VLA (20, 21)	10 52	57 29	6, 20 cm	0.35, 0.09	11, 30 μJy
		SIRTF/GTO (12, 13)			3.6–160 μm	0.4	0.11 mJy[e]
		SCUBA 8 mJy (22, 23)	10 52	57 22	450, 850 μm	130 arcmin²	8 mJy
		VLA (24)			20 cm	100 arcmin²	5 μJy
		SCUBA/SHADES (6)			450, 850 μm	0.25	60, 3 mJy
	LH-W (19)	*ISO*	10 34	58 00	90, 175 μm	0.5	15 mJy
		Chandra (25)	10 34	57 40	0.5–8 keV	0.4	40, 70 ks
ELAIS N1	ELAIS (1)	*ISO*	16 10	15 31	15, 90, 175 μm	2.6	1 mJy[b]
	FIRBACK (26)	ISOPHOT	16 11	54 25	170 μm	1.98	50 mJy
	ELAIS Deep X-Ray Survey (27)	*Chandra*	16 10	54 33	0.5–8 keV	300 arcmin²	75 ks
		XMM			0.5–10 keV	1.2	30 ks
ELAIS N2	ELAIS (1)	*ISO*	16 37	41 16	7, 15, 90, 175 μm	2.6	1 mJy[b]
	FIRBACK (26)	ISOPHOT	16 36	41 05	170 μm	0.96	50 mJy
	SCUBA 8 mJy (22, 23)	SCUBA	16 37	41 02	450, 850 μm	130 arcmin²	8 mJy
		VLA (24)			20 cm	100 arcmin²	9 μJy
	ELAIS Deep X-Ray Survey (27)	*Chandra*	16 36	41 01	0.5–8 keV	300 arcmin²	75 ks
		XMM			0.5–10 keV	1.2	30 ks

NOTE.—Units of right ascension are hours and minutes, and units of declination are degrees and arcminutes.

[a] ks for X-ray, limiting magnitude for optical/NIR, ~1 σ flux density for IR-radio, neglecting confusion noise.

[b] 15 μm.

[c] *R/r/r′* band.

[d] 24 μm.

[e] 3.6 μm.

REFERENCES.—(1) Oliver et al. 2000; (2) Alexander et al. 2001; (3) Gruppioni et al. 1999; (4) http://xmm.vilspa.esa.es; (5) Mizumoto et al. 2003; (6) Dunlop et al. 2003, http://www.roe.ac.uk/ifa/shades; (7) Cohen et al. 2003; (8) Giacconi et al. 2001; (9) Rosati et al. 2002; (10) Schreier et al. 2001; (11) http://www.stsci.edu/ftp/science/goods; (12) Fazio et al. 2003; (13) Rieke et al. 2003; (14) Hasinger et al. 1998; (15) Hasinger et al. 2001; (16) Kenter, Murray, & Meehan 2002; (17) Fadda et al. 2002; (18) Rodighiero et al. 2003; (19) Kawara et al. 1998; (20) Ciliegi et al. 2003; (21) de Ruiter et al. 1997; (22) Scott et al. 2002; (23) Fox et al. 2002; (24) Ivison et al. 2002; (25) Yang et al. 2003; (26) Dole et al. 2001; (27) Manners et al. 2003.

sources. The second coverage is offset in the cross-scan direction by 150″ to provide additional 160 μm Ge:Ga array redundancy and counteract the memory effects present in the 70 μm Ge:Ga array.

Several AORs are required in each of the two coverages. The adjacent AORs in each coverage overlap by 70″. This will prevent gaps if adjacent AORs are rotated by less than about 0°.5 relative to each other (corresponding to about a day at our high ecliptic latitudes).

Table 6 gives details of the MIPS AORs.

2.2.3. Other Considerations

Since *SIRTF* observes with only one instrument at a time, our IRAC and MIPS observations will be separated by several
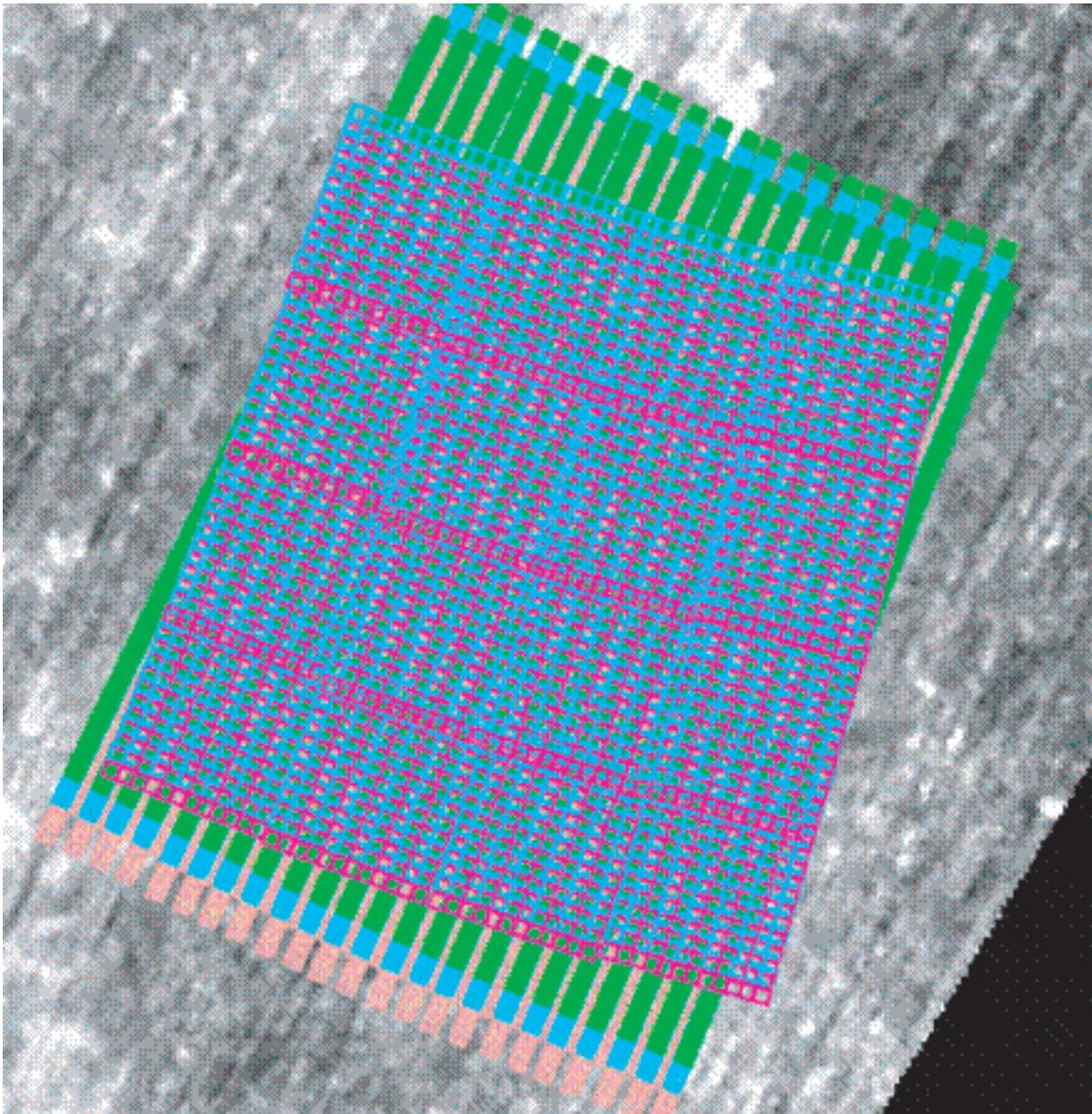
FIG. 3.—Visualization of the MIPS (*green*) and IRAC (*blue and magenta*) AORs for the ELAIS S1 field. The AORs have been rotated for MIPS observations occurring over 5 days, and the IRAC observations spread over 10 days. The map in the background is the *IRAS* ISSA map at 100 μm.

days, at least. This will result in a relative rotation of a few degrees overall between the MIPS and IRAC maps.

In the Lockman and *Chandra* Deep Field–South (CDF-S) fields, the SWIRE observations overlap deeper GTO surveys. Our AORs will be "segmented" into smaller regions in the areas of overlap, and the resulting small AORs that overlap the GTO regions will be embargoed during the GTO proprietary period. Details of the embargoed areas are not yet available because they depend on exactly when the SWIRE and GTO observations are made by *SIRTF*. When details become available, they will be provided on the SWIRE public Web pages.

2.3. Supporting Observations and Data Sets

2.3.1. Optical and NIR Imaging

Ground-based optical/near-infrared imaging data for the SWIRE fields will be essential to do the following:

1. Obtain optical identifications for the roughly 2 million IR sources predicted to be detected by SWIRE. The present statistics on faint *ISO* sources in the HDFs indicates that on the order of 90% of the SWIRE MIPS sources could be detected to *V*, *R* ~ 25; at the same limits, and on the basis of *K*-selected

TABLE 5
IRAC FIELD SIZES AND AOR COVERAGES

| | EACH AOR (grid of images) | | FIELD LAYOUT (grid of AORs) | |
FIELD	cols × rows	deg × deg	cols × rows	deg × deg
ELAIS S1	12 × 13	0.94 × 1.02	4 × 4	3.62 × 3.94
XMM-LSS	13 × 13	1.02 × 1.02	3 × 3	2.95 × 2.95
CDF-S	10 × 13	0.78 × 1.02	3 × 3	2.23 × 2.95
Lockman	12 × 13	0.94 × 1.02	4 × 4	3.62 × 3.94
Lonsdale	12 × 11	0.94 × 0.86	3 × 3	2.71 × 2.47
ELAIS N1	13 × 13	1.02 × 1.02	3 × 3	2.95 × 2.95
ELAIS N2	11 × 16	0.86 × 1.25	2 × 2	1.65 × 2.43

samples in the HDF-N, 80% of the IRAC sources may be detected.

2. Provide photometric redshifts for SWIRE sources. Three-color optical photometry will be essential to supplement IRAC photometry for high-quality photometric redshift estimation (see § 5.1). IRAC colors alone are powerful for stellar populations owing to the H^- opacity feature at 1.6 μm (Simpson & Eisenhardt 1999); however, they suffer at $z < 1.5$ because of the degeneracy of the stellar population with age and confusion by the 2 μm CO bandheads (Sawicki 2002). For star-forming galaxies, MIPS colors are limited for photometric redshifts because there is great variation in the $\lambda > 10$ μm SEDs of galaxies, where dust emission dominates. However, three-color optical, coupled with IRAC ($\lambda_{rest} < 5$ μm) photometry, yields good photometric redshift discrimination.

3. Provide colors and rough morphologies for source classification and the study of the effects of environment on morphology.

4. Optimize the discovery of rare sources—e.g., high-z, high-L, and oddball SEDs—which require good optical imaging for identification and follow-up; SWIRE has sensitivity to objects as rare as 1 in 10^6.

5. Produce independent optical samples for comparison with IR-selected samples.

The original goal for optical/near-infrared ground-based imaging in the SWIRE survey fields was to obtain multicolor optical imaging (SDSS g', r', i', or equivalent) down to the median optical magnitude ($r' \sim 25$) and galaxy redshift ($z \sim 1$) for the entire SWIRE survey area with as much complementary near-infrared (J, K') data as could be obtained. Despite extensive observational facilities available to the project at NOAO (KPNO/CTIO Mosaic Cameras, 2.1 m FLAMINGOS), Palomar (LFC, WIRC), ESO (2.2 m WFI, VLT VIMOS), INT (WFS), etc., as well as existing data for our ELAIS survey fields, this goal has proved difficult to meet. Moderate-depth $R/r' \sim 24$–25 data will be available for most of SWIRE's $\sim$65 deg^2, with a variety of additional imaging available with other filters and to greater depths. The available and projected ground-based imaging data that will become accessible to the astronomical community are summarized by field in Table 7.

NOAO: KPNO and CTIO Mosaic Imaging.—Time has been granted under the NOAO-*SIRTF* observing program through the original SWIRE proposal for optical imaging in CDF-S, Lockman, and Lonsdale using the Cerro Telolo Inter-American Observatory (CTIO)/Kitt Peak National Observatory (KPNO) Mosaic Cameras. The Mosaic Cameras image $0°.6 \times 0°.6$ in a single filter with scale $0''.26$–$0''.27$ pixel^{-1}. Imaging has been obtained to a range of depths, as summarized in Table 7.

Palomar LFC.—Further imaging in Lockman and Lonsdale is being obtained at Palomar Observatory using the 5 m Hale telescope and its Large Format Camera (LFC; Simcoe et al. 2000). The Palomar LFC has a field of 0.13 deg^2 with $0''.18$ pixel^{-1}, which may be binned to $0''.36$ pixel^{-1} for less-than-optimal seeing.

INT.—A strong motivation for selecting fields from the ELAIS survey regions was the availability of ground-based imaging data as well as the original *ISO* survey observations. In particular, the ELAIS N1 and N2 fields have been imaged through the Isaac Newton Telescope's Wide Field Survey (INT WFS)[24] covering nearly the entire SWIRE EN1 and EN2 fields. Details of the overlap between the INT WFS and *SWIRE* will depend upon *SIRTF* scheduling.

Further INT Wide Field Camera (INT WFC) observations in r' have been undertaken by S. Oliver, E. Gonzalez, and M. Salaman at the University of Sussex (ISLES program). The

---

[24] http://www.ast.cam.ac.uk/~wfcsur/index.php.

TABLE 6
MIPS FIELD SIZES AND AOR COVERAGES

Field	Legs per AOR	Cross-Scan Size per AOR (deg)	AORs per Coverage	Cross-Scan Extent (deg)	Scan Length (deg)
ELAIS S1	4	0.32	12	3.58	4.0
XMM-LSS	5	0.39	8	3.00	3.0
CDF-S	4	0.32	8	2.38	3.0
Lockman	4	0.32	12	3.58	4.0
Lonsdale	6	0.47	6	2.68	2.5
ELAIS N1	5	0.39	8	3.00	3.0
ELAIS N2	6	0.47	4	1.78	2.5

TABLE 7
GROUND-BASED IMAGING

FIELD	TELESCOPE/INSTRUMENT	FILTERS AND MAGNITUDES (Vega, 5 σ, 3″)								AREA COVERED [PROJECTED][a] (deg^2)
		u' [U]	g' [B]	v' [V]	r' [R]	i' [I]	z' [Z]	J [H]	K [K_s]	
ELAIS S1	ESO 2.2 m/WFI	...	[26]	[25.5]	[25.5]	...	...	...	...	[6.25]
	ESO VLT/VIMOS	...	...	...	...	[25]	[24]	...	...	[6.25]
XMM-LSS	CFHT/Megacam[b]	25.5	26.5	...	25.7	25.5	24.0	...	...	[64]
	Palomar 5 m/LFC	...	...	25	...	...	...	...	...	0.5
	UKIRT/WFCAM[c]	...	...	...	...	...	...	22.5	21	[8.75]
CDF-S	CTIO 4 m/Mosaic II	24	25.7	...	25	24	23.5	...	...	1.6 [7]
	CTIO 4 m/Mosaic II	[27]	27	...	26.5	25.8	...	...	...	0.36
	Las Campanas/WIRC	...	...	...	...	...	...	...	$K' = 20.5$	0.6 [1.0]
Lockman	KPNO 4 m/Mosaic I	...	25.7	...	25	24	...	...	...	2.0 [4]
	KPNO 4 m/Mosaic I	...	26.7	...	26	25	...	...	...	0.36
	KPNO 2.5 m/Flamingos	...	...	...	...	...	...	...	$K' = 19.5$	0.09
	Palomar 5 m/LFC	...	25.7	...	25	24	...	...	...	1.5
	INT/WFC (ISLES)	...	...	...	23.8	...	...	...	...	9.2
	Palomar 5 m/WIRC	...	...	...	...	...	...	21	[20]	[1.0]
	UKIRT/WFCAM[c]	...	...	...	...	...	...	22.5	21	[8.75]
Lonsdale	KPNO 4 m/Mosaic I	...	25.7	...	25	24	...	...	...	0.7
	INT/WFC (ISLES)	...	...	...	23.8	...	...	...	...	6.5
ELAIS N1	INT WFS	[23.3]	24.7	...	23.8	23.0	[21.7]	...	...	9.0[d]
	UKIRT/WFCAM[c]	...	...	...	...	...	...	22.5	21	[8.75]
ELAIS N2	INT WFS	[23.3]	24.7	...	23.8	23.0	[21.7]	...	...	4.5[d]

[a] Based on time allocated or programs already approved.

[b] The CFH Legacy Survey, http://www.cfht.hawaii.edu/Science/CFHLS (AB magnitudes).

[c] UKIDSS.

[d] Overlap between SWIRE area and INT fields depends on field orientation.

goal of ISLES is to ensure complete $r' \sim 24$ coverage of the SWIRE northern fields, with deeper imaging over smaller central fields.

ES1-ESIS.—In the ELAIS S1 field, the ESIS[25] program is being carried out by A. Franceschini and colleagues at the University of Padova. ESIS is an optical imaging survey over ~6 deg^2 in five bands based on the ESO WFI 2.2 m and VIMOS to $\sim$25–26 mag. The total amount of observing time will be 27 nights with the 2.2 m WFI and eight nights with VIMOS.

XMM-LSS.—The full $8° \times 8°$ *XMM*-LSS area is being imaged by CFHT's MegaCam as part of the Canada-France-Hawaii Legacy Survey. Additionally, a large consortium of observatories and instruments are supporting further ground-based observations, including NOAO, Subaru, and ESO. These data will be available to the community via CFH Legacy Survey and the *XMM*-LSS Consortium. Their ground-based program is summarized at the *XMM*-LSS Web site.[26]

The VIRMOS Deep Imaging Survey has imaged ~4 deg^2 in *BVRI* to $I_{AB} = 24.8$ and 1.4 deg^2 to $I_{AB} = 25.3$, with spectroscopy to $I_{AB} = 22.5$ and $I_{AB} = 24$, respectively, to follow (Le Fevre et al. 2003). Also covering part of the SWIRE/*XMM*-LSS field is the NOAO Deep-Wide Survey in *BRIJHK*, reach-

ing 26 mag in *R* and 21.4 in *K* (Jannuzi et al. 2002). Depending on orientation of the SWIRE field, the overlap will be about ~2 deg^2.

2.3.2. Near-Infrared Imaging

FLAMINGOS imaging of the SWIRE Lockman field in K' using the KPNO 2.1 m telescope was obtained in 2001 December and 2002 February. Poor weather restricted observations to a total of eight pointings of 0.09 deg^2 (0″6 pixels) to a limiting magnitude $K' \sim 19.5$. Deeper near-infrared observations in the Lockman field were carried out in 2003 February using the Cornell Wide-Field Infrared Camera on the 5 m telescope at Palomar by G. Stacey et al.

A survey is being conducted by A. Cimatti in ELAIS S1 to $J = 22$ and $K = 20$ over 1 deg^2 using the ESO 3.5 m NTT/SOFI. Approximately half of the observations have been carried out with the remainder to be completed by the end of 2003.

The 2MASS survey covers the entire SWIRE survey area. In the SWIRE Lockman Hole field, a unique 2MASS deep survey exists (Beichman et al. 2003); ~1 mag deeper than the main 2MASS survey, the 24 deg^2 area overlaps most of the planned SWIRE Lockman Hole field (dependent on the final orientation of the SWIRE/*SIRTF* observation) and includes

[25] ESO-*SIRTF* Wide-Area Imaging Survey, http://dipastro.pd.astro.it/esis.

[26] http://vela.astro.ulg.ac.be/themes/spatial/xmm/LSS/opt_fu_e.html.

69,115 sources to 90%–95% completeness levels of 17.8, 16.5, and 16.0 at J, H, and K_s.

A United Kingdom consortium, the UKIRT Infrared Deep Sky Survey (UKIDSS),[27] is planning to observe 8.75 deg^2 in each of three SWIRE fields as part of their Deep Extragalactic Survey. Using UKIRT's Wide Field Infrared Camera (WFCAM; 0.19 deg^2 field of view, 0″.4 pixel^{-1}), UKIDSS will begin by covering approximately 3 deg^2 in each of Lockman, *XMM*-LSS, and EN1 to $J = 22.5$ and $K = 21$ in the first 2 years. Subsequent observations will complete the J and K imaging over 8.75 deg^2 and will image a smaller area to $H \sim$ 22. WFCAM is due to be commissioned in late 2003, and the UKIDSS Deep Extragalactic Survey will require 118 nights over 7 years.

2.3.3. Optical and NIR Data Processing

The bulk of the new imaging data reduction has been or is being carried out at the Cambridge (UK) Astronomical Survey Unit (CASU) via their image reduction pipeline, led by M. Irwin. The ELAIS N1 and N2 INT data have been fully processed at CASU. KPNO, CTIO, and Palomar observations of SWIRE's CDF-S, Lockman, and Lonsdale fields are also being carried out through the CASU pipeline under supervision of M. Rowan-Robinson and colleagues at Imperial College.

ESO observations by the Padova group and INT observations by the Sussex group are being reduced by the groups themselves.

Source extraction for all optical and NIR imaging is being undertaken in a uniform manner at IPAC, using SExtractor (Bertin & Arnouts 1996) and following the procedures described for SWIRE/IRAC data processing and validation. Details will be provided in a forthcoming publication.

2.3.4. ISO Mid-IR Surveys in the ELAIS Fields

Roughly 4 deg^2 in each of the ELAIS N1, N2, and S1 fields have been observed with the *ISO* at 15 and 90 μm (Oliver et al. 2000). Lari et al. (2001) and M. Vaccari et al. (2003, in preparation) report $\sim$2000 cataloged 15 μm sources in these areas. These samples appear to be complete for fluxes brighter than $S_{15\,\mu m} \simeq 1.5$ mJy and include sources down to $\simeq$0.8 mJy. Although much shallower than the planned SWIRE observations, these data may prove useful to complement the SWIRE photometry between 8 and 24 μm.

2.3.5. A Deep Radio Survey in the Lockman Hole

We have conducted an ultradeep A/C/D-array VLA imaging survey at 20 cm, centered at 10^h46^m, $+59°01'$ and reaching $\sim$3 μJy rms (F. Owen et al. 2003, in preparation), which matches the deepest ever VLA imaging. This field was picked to be the best place in the entire $\sim$65 deg^2 SWIRE Legacy survey for

such a deep survey, with respect to elevation, and brighter radio sources in the primary beam and side lobes. The goals are to determine if and how the radio-FIR relation evolves with redshift (Compton losses might be expected to increase with z, for example), to determine whether AGNs and star formation are more closely connected at higher z, and to identify populations of heavily obscured AGNs. The radio image is extremely well matched in depth to SWIRE; we expect to detect more than 90% of the SWIRE population and to measure evolution of the star formation rate out to $z = 1–3$ with a sensitivity equivalent to $\sim$10 $M_\odot$ yr^{-1} at $z \sim 1$ and $\sim$200 $M_\odot$ yr^{-1} at $z \sim 3$ (if the local radio/IR correlation holds). This radio survey is not in the same location as previous *ROSAT*, *ISO*, SCUBA, *Chandra*, and *XMM* surveys in the Lockman Hole area because those fields are not as optimal for deep radio imaging (see Table 4).

2.3.6. Broader Radio Imaging

It would be highly desirable to image the SWIRE area deeply in the radio but impractical with current VLA capabilities to match SWIRE depth over an appreciable fraction of the VLA-accessible SWIRE areas, a total of about 43 deg^2. However, a VLA survey with 5″ FWHM resolution and 40 μJy rms noise at 1.4 GHz could yield a complete catalog of $\sim$2.5 $\times$ 10^4 radio sources stronger than 200 μJy. This is substantially deeper than the FIRST survey and would detect on the order of 13% of the SWIRE MIPS sources, about 14,600 total, according to the models of Xu et al. (2003). Most of these sources would be star-forming galaxies obeying the remarkably tight FIR/radio correlation, and the sample would also include many radio-loud AGNs. The FIRST survey itself overlaps $\sim$34 deg^2 of the SWIRE area (Lockman, Lonsdale, ELAIS N1, and ELAIS N2) and might be expected to detect $\sim$850 SWIRE sources. For comparison, Ivezic et al. (2002) estimate about 1350 SDSS-FIRST sources within the boundaries of the SWIRE fields, about 200 of which are radio-loud quasars.

Gruppioni et al. (1999) have observed 4 deg^2 of the ELAIS S1 field with the Australia Telescope Compact Array at 1.4 GHz, to a sensitivity of $\sim$80 μJy and with a resolution of 8″ $\times$ 15″, detecting about 600 sources.

Cohen et al. (2003) present results of a VLA A-array 74 MHz survey of the entire *XMM*-LSS field, including the subset to be observed by SWIRE, with flux limits of 275 mJy beam^{-1}, resolution of 30″, and source density of 2 deg^{-2}. They also present 325 MHz VLA A-array imaging of 5.6 deg^2 to 4 mJy beam^{-1} with a resolution of 6″.3 and a source density of 46 deg^{-2} (see Table 4).

2.3.7. X-Ray Imaging

The *XMM*-LSS survey will have a sensitivity of $\sim$3 $\times$ 10^{-13} ergs s^{-1} cm^{-2} for point sources and $\sim$10 ergs s^{-1} cm^{-2} for extended sources in the 0.5–2 keV band. The SWIRE area will be covered by an $\sim$9 $\times$ 9 grid of 10 ks *XMM*/EPIC pointings

---

separated by $20'$. Also within the SWIRE/*XMM*-LSS field are (1) the Subaru/*XMM-Newton* Deep Survey (see Table 4), which covers 1 deg^2 with 7×50 ks pointings and one 100 ks pointing (Mizumoto et al. 2003),[28] and (2) most of two *XMM* medium depth surveys (P.I.s K. Mason and M. Watson), which cover a total of $\sim$2 deg^2 with a mean exposure time of 20 ks.

A mosaic of four deep (100 ks) integrations with *XMM-Newton* (P.I. Fabrizio Fiore) has been approved in AO2 to cover 1 deg^2 in ELAIS S1. With this survey, flux limits of 2×10^{-15}, 3×10^{-15}, and 3×10^{-16} ergs s^{-1} cm^{-2} will be reached in the 2–10, 5–10, and 0.5–2 keV bands, respectively.

3. SKY SIMULATIONS

Simulations are used extensively by SWIRE, both for predicting the SWIRE source populations and thereby constraining the cosmological models once the data are available, and to validate the SWIRE pipeline data reduction and source extraction process, which is complex and involves numerous non-linear components. Understanding the behavior of this pipeline can be accomplished only by generating simulated data sets with known inputs and examining the resulting output. Metrics examined include the completeness and reliability of extracted sources, accuracy of band-merging of multiple wavelengths, effective beam shape, and accuracy of derived positions.

The sky simulations have three ingredients: model source populations, truth images reflecting the expected band-dependent instrumental PSFs, and full image reconstructions taking into account the observing parameters of the SWIRE survey and the expected instrumental effects. We describe each step in turn below.

The SWIRE sky simulator can generate images with a range of tunable parameters. Here we describe a simulation that is tuned to a specific $\sim$0°5 × 0°5 SWIRE field in the Lockman Hole. It has three model components—galaxies, stars, and cirrus—which are described in turn below. The model star and galaxy source populations were derived from the actual positions of real stars and galaxies detected within this field in an $r'_{lim} \sim$ 26.7 image. Source extractions were done using SExtractor, and stars were separated from galaxies using a stellarity index (a measure of difference in FWHM from the PSF) of less than 0.7. A model star or galaxy was matched to each real source by r' magnitude, and model sources predicted to have an r' magnitude too faint to be visible on the image were assigned a random position within the image.

3.1. Source Populations

Both dusty galaxies and E/S0s, the latter to be detected presumably only in the IRAC bands, have been simulated using the models of Xu et al. (2003). Models S1, S2, and S3 for dusty galaxies exploit a large library of SEDs of 837 local IR galaxies (*IRAS* 25 μm selected) from the UV (700 Å) to the

radio (20 cm), including *ISO*-measured 3–13 μm unidentified broadband features (unidentified infrared bands [UIBs]). The basic assumption is that the local correlation between SEDs and mid-infrared (MIR) luminosities can be applied to earlier epochs of the universe. By attaching an SED appropriately drawn from the SED library to every source predicted according to the evolved luminosity functions, the algorithm enables comparison with surveys in a wide range of wave bands simultaneously. Therefore, the model parameters are tightly constrained by available surveys in the literature. Three populations of dusty galaxies are considered in the model: (1) normal late-type galaxies, (2) starburst galaxies, and (3) AGNs, each with a different evolutionary function. In models S1 and S3, most of the increase in IR luminosity density to early times is attributed to starbursts, while in S2 a large fraction is attributed instead to quiescent star formation in galaxy disks or cirrus emission. The predictions of these models for the global star formation rate as a function of redshift are compared with observations in Figure 9 of Xu et al. (2003). All models adequately fit all available optical, near-, mid-, and far-IR, submillimeter, and radio number counts, redshift distributions, and the CIB, although each has its shortcomings (Xu et al. 2003). We have chosen model S3 as the best overall representation of the IR universe for most of our predictions discussed in § 6, but we used model S1, which has the highest FIR count rates of the three models, for constructing the simulated images in order to provide a conservative upper limit to the confusion noise we will likely encounter on the sky.

Model E2, for E/S0 galaxies, follows a simple passive evolution approach. The basic assumption is that there has been no star formation in an E/S0 galaxy since its initial formation. Consequently, its radiation in different bands (i.e., the SED and the L/M ratio) evolves passively with the ever-aging stellar population. Instead of assuming that all E/S0 galaxies formed at once together (as in the classical monolithic galaxy formation scenario), the E/S0 galaxies are assumed to form in a broad redshift range. The dependence of the formation rate of E/S0 galaxies to the cosmic time is assumed to be a truncated Gaussian function, specified by a peak formation redshift $z_{peak} = 2$, an e-folding formation timescale $\omega = 2$ Gyr, and a starting redshift $z_0 = 7$. SEDs of E/S0 galaxies of different ages are calculated using the code GRASIL (Silva et al. 1998). Note that this model is intended to roughly approximate the hierarchical merging of systems in a CDM prescription but should not be considered a full CDM treatment; an independent modeling effort addresses SWIRE predictions in a CDM-based scenario (F. Fang et al. 2003, in preparation).

In Figure 8, predicted redshift distributions in six SWIRE/*SIRTF* bands models are presented. Color-color distributions are shown in Figure 9. For these figures, we use the SWIRE 5 σ photometric sensitivity limits for 3.6–24 μm and the confusion limits of the Rowan-Robinson (2001) model at 70 and 160 μm (see Table 3).

The stars in the SWIRE simulation are based on point sources
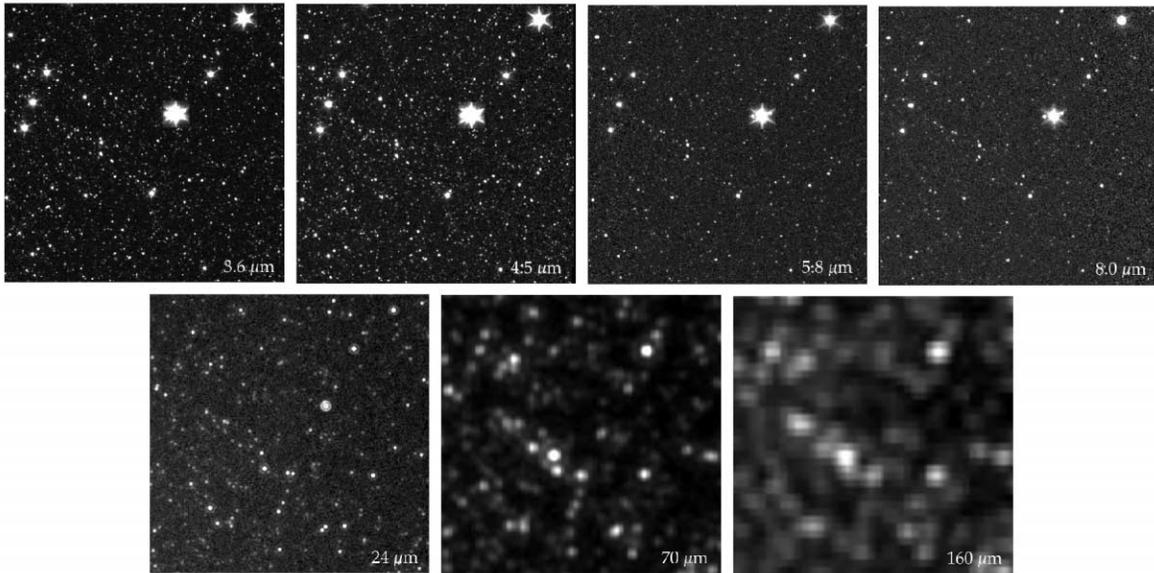
---

[28] http://www.naoj.org/staff/chris/SXDS.

FIG. 4.—Simulated full-depth SWIRE images, 10′ on a side, in each of the seven *SIRTF* bands.

(stellarity greater than 0.7) identified in the Lockman r'-band image. The distribution of spectral types and luminosities for the simulated stars was generated using a 2MASS stellar population model developed by T. Jarrett (Jarrett, Dickman, & Herbst 1994; Cambresy et al. 2002). Once assignments of spectral class were made, the K-band brightness of the star was calculated using the $(r'-K)$ versus spectral and luminosity class from the model. Finally, stellar fluxes in the IRAC and MIPS filters were predicted using a blackbody extrapolation from the K band to the mid- and far-IR bands.

To properly assess the impact of cirrus on our observations, we have simulated the cirrus in each of the SWIRE fields. To do this, we add synthetic cirrus at a higher resolution to the real low-resolution cirrus maps that we have from *IRAS*. The synthetic cirrus is cloned from real low-resolution maps of a larger area of sky and "shrunk" to our field size and resolution requirement. Cloning, shrinking, and adding the synthetic data to the real data is done to produce a map whose power spectrum matches an extrapolation of the real power spectrum. This method is described in more detail by S. Oliver et al. (2003, in preparation).

3.2. Truth and Simulated Images

The truth-image generator uses the instrument PSF, provided by the *SIRTF* Science Center (SSC), to place sources from a model, such as that described above, onto a "truth" image. The PSFs are theoretical PSFs based on the measured, as-built *SIRTF* optical train, including all expected optical aberrations, and are expected to be very similar to the in-flight performance. They are quantized with pixels typically 4–8 times smaller than the actual instrument pixels and extend to many tens of beam widths. There is no time dependence, but unlike *HST* (which has Sun-induced "breathing" modes), there is no a priori expected time variance to the *SIRTF* PSF. The truth-image generator can create random positions when they are missing in the source list, as is the case for model sources fainter than the r' limit of the Lockman field image. For galaxies, correlated positions can also be made on the basis of a predicted two-point angular correlation function.

In the simulation of the Lockman field illustrated in Figures 4 and 5, the optical detections of stars and galaxies in a 0.25 deg² area were matched in r-band flux with model sources to yield 36,271 galaxies and 1356 stars with positions and IRAC and MIPS fluxes. The truth-image generator also generated 292,746 random positions for fainter "unmatched" galaxies from the model. The truth-image pixels are upsampled by a factor of 4 in each dimension, giving pixel sizes of 0″.30 for IRAC and 0″.64, 2″.46, and 4″.00 for MIPS 24, 70, and 160 μm truth images, respectively. The instrument PSF was further upsampled so that a source is placeable to $\frac{1}{8}$ of the truth-image pixel, or 1/32 of the instrument pixel in both dimensions. For computing efficiency, the central $\frac{1}{8}$ of the PSF image is used for sources fainter than 1 mJy. The separate cirrus frames are then combined to yield the final truth images. The total number of model sources in the simulation that we would expect to detect in one or more SWIRE bands is 24,500 (5 σ photometric sensitivity at 3.6–24 μm; confusion limits at 70 and 160 μm).

The IRAC simulated images, calibrated in units of surface brightness, were generated from the truth images using the IRAC Science Data Simulator (Ashby, Surace, & Hora 2003). The command files produced by the *SIRTF* Planning Observation Tool (SPOT) were used to produce a simulation of the
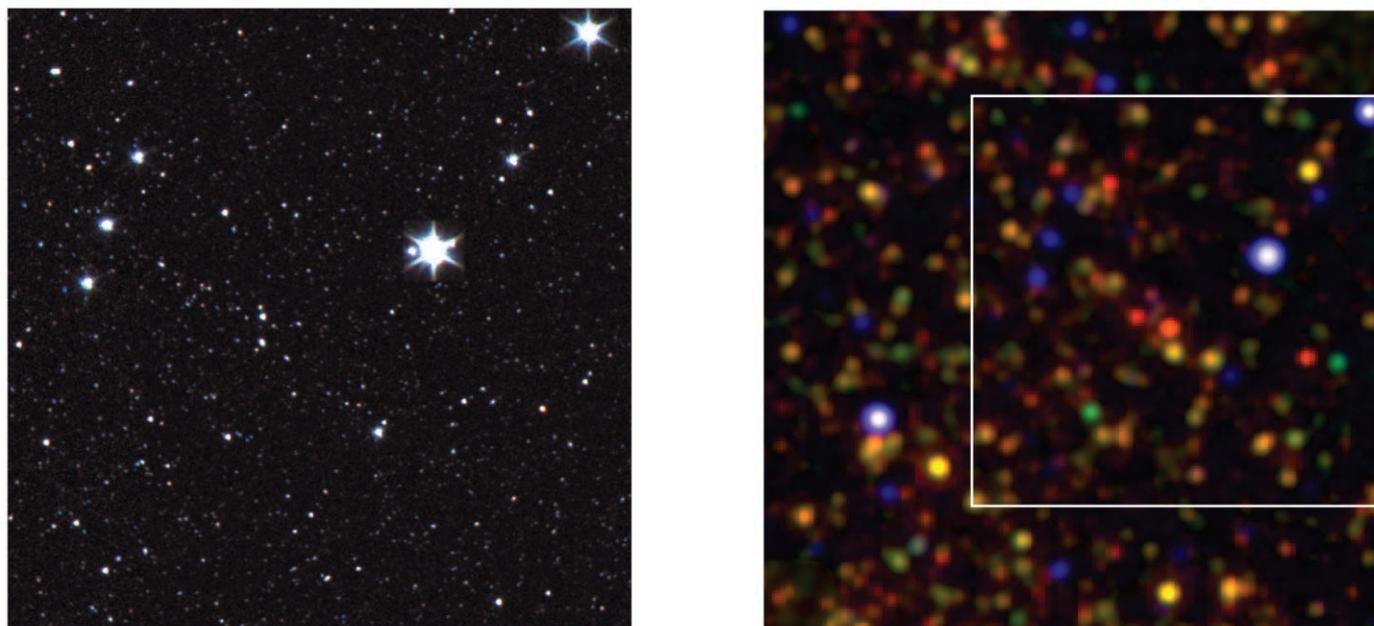
Fig. 5.—Pseudo–true-color images constructed from simulated IRAC data at 3.6, 4.5, and 5.8 μm, 10′ on a side (*left panel*) and IRAC/MIPS data at 8, 24, and 70 μm, 15′ on a side, with the coverage of the IRAC three-color image outlined (*right panel*). The images are made from simulated detector data using the actual SWIRE observation parameters and then mosaicked with the SWIRE pipeline using Montage (see text). The data have been smoothed to the spatial resolution of the longest wavelength for the purpose of co-addition.

IRAC data-taking process, including simulated slews using the commanded pointing and all detector effects such as the flat-field response, nonlinearity, etc. Generally, most simulations are generated to mimic the form of the reduced, calibrated data that will be provided by the SSC. In this form, the simulations are individual IRAC images with the expected sensitivity and noise properties of IRAC.

The MIPS simulations were made with a modified version of the WIRE science image simulator (Shupe, Huber, & Hacking 1996). Owing to the complex behavior of the Ge detectors and the on-board data-taking procedures, our simulation efforts have focused on producing the basic calibrated images, in units of surface brightness. Read noise and photon noise are simulated, and the simulated pixels are scanned across the truth images in the manner planned for MIPS scan maps.

4. DATA PROCESSING AND PRODUCTS

4.1. Data Processing

SWIRE data processing consists primarily of five steps: organizing and tracking the data, mosaicking/co-addition, source extraction, band merging, and catalog building. The SWIRE data system is designed under a Sun UNIX environment. As much as possible, existing off-the-shelf software has been used to reduce development time and costs and take advantage of well-understood software properties and community support. Architecturally, the software consists of individual modules executable from a UNIX command line and connected via

PERL wrapper scripts. Additional PERL modules perform various housekeeping functions such as file transfer and reformatting. Commercial database software administrated by the Infrared Science Archive (IRSA) at IPAC is used for tracking each individual observation. Furthermore, the generated data products such as source catalogs are loaded into a database that is accessible from the IRSA data system, allowing use of their advanced search and data-mining tools. A Web-based interface is used for most functions that require interaction with the SWIRE science team.

After receipt from the Deep Space Network, the SSC performs an initial processing of the data. Automated pipelines remove nearly all known instrumental signatures from the data. These include but are not limited to dark current subtraction, flat fielding, bias removal, cosmic-ray detection, and image latent tracking. Additionally, the SSC performs basic calibration tasks, notably flux calibration (in units of surface brightness) and pointing reconstruction. The result of this processing is known as basic calibrated data. It is with these data that the SWIRE pipelines normally begin their processing.

Data (both raw instrumental data and calibrated data) are initially received in the SWIRE data system in a tar bundle sent by the SSC. A daemon process running within the data system automatically unpacks this data upon its arrival and stores it in a terabyte disk array. The data are registered by the daemon into a science operations database, which stores its location within the system, its header contents, its current pro-
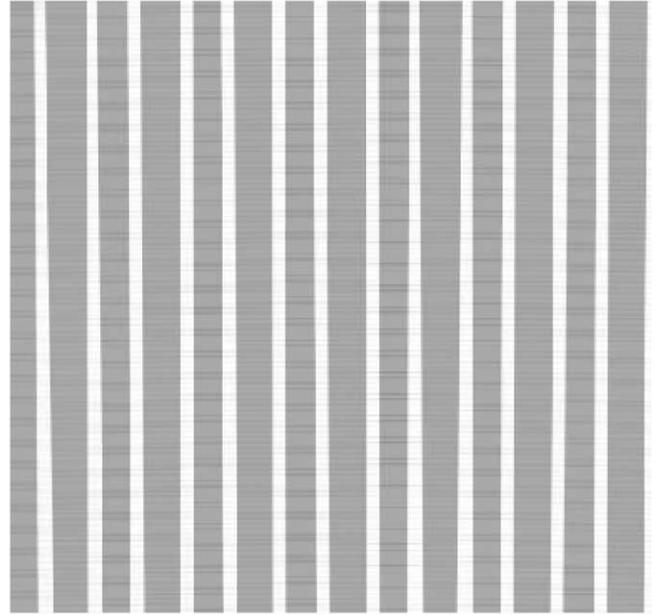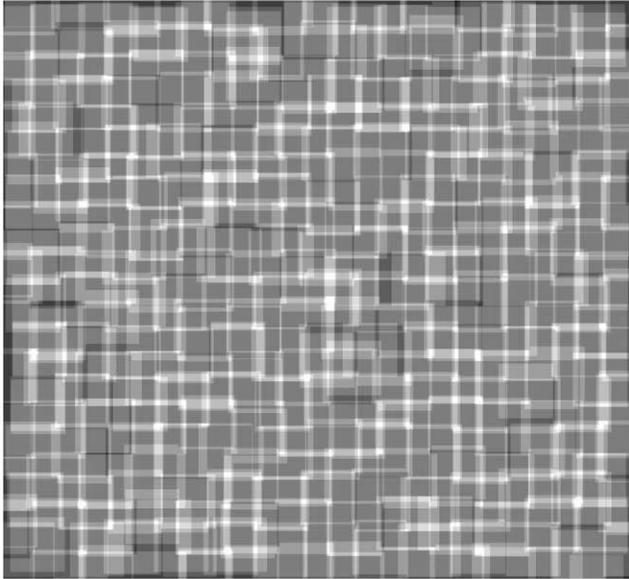
FIG. 6.—Simulated full depth coverage map of a 1.0×1.0 deg^2 IRAC 3.6 μm image (*left panel*) and a 0.6×0.6 deg^2 MIPS 70 μm image (*right panel*). Lighter areas indicate deeper coverage.

cessing status, and various statistics about the pixel contents. If needed, frame-level reprocessing of the raw data into calibrated data, using the SSC pipeline within the SWIRE system, is performed. This reprocessing is likely to be needed during the early mission when the instrument calibration is changing rapidly. Later in the mission when the calibration and data reduction have stabilized, this will become unnecessary. Web pages are automatically generated that present thumbnail images and statistics for every image received, along with direct access to the original images and on-line analysis tools. Team members are then contacted via an automated system to perform quality analysis checking from their remote institutions. The team members connect to the SWIRE server, examine the data, and submit an evaluation of the data quality. Data quality is assessed by both qualitative and quantitative guidelines. A set of basic quantitative statistics are used to provide a lower level of basic data rejection. In addition to these quantitative pass/fail criteria, all the data are examined by eye for unknown or unanticipated defects (for example, unexpected time variability). When such a defect is found, it is handled on a case-by-case basis. When sufficient data graded of high quality have accumulated for a given SWIRE field, SWIRE pipeline processing is initiated.

The individual frames are then processed in groups, with corrections made to individual frames on the basis of the behavior of the data group. This allows for correction of time-dependent effects, such as drifts in the background bias level, which is a known effect in IRAC data. This is also expected to be a major step in the processing of MIPS data, as the MIPS

germanium detectors exhibit numerous transient effects. In essence, this step will result in destriping of the data and elimination of large-scale detector-based variability.

At this point, the data are still in the form of individual images, one per telescope pointing. The data will be reprojected onto a common TAN-TAN spatial projection (one per each of the seven SWIRE fields). At the same time, detector distortion is corrected. Reprojection is done via the Montage software.[29]

Predefined tiles one-half degree on a side are then generated by co-adding all of the reprojected data lying within the specified tile. Outlier detection (e.g., cosmic rays) is performed by examining the contribution from each input pixel to a given output pixel and identifying high-σ outliers. The data are then co-added using Montage onto a reprojected grid finer than the original data scale to minimize aliasing with the large detector pixels. Coverage maps for 1 deg^2 IRAC and MIPS mosaics are shown in Figure 6.

After co-addition, sources are detected in the co-added and mosaicked tiles. Source densities are expected to be on the order of 100 sources per 5′ frame in our densest IRAC filter (3.6 μm). This source density is similar to or less than the confusion limit. For these data, we are using the SExtractor software written by Emmanuel Bertin. This reads the co-added

---

[29] Montage (http://montage.ipac.caltech.edu) is an image mosaic service under development by the Center for Advanced Computing Research, California Institute of Technology, the Infrared Processing and Analysis Center, California Institute of Technology, and the Jet Propulsion Laboratory. The images presented here were derived with an evaluation version of Montage.

data and weight images generated during the mosaicking process, detects sources, and performs aperture and isophotal photometry. For objects identified as point sources, extracted circular aperture photometry is used, to which is applied an aperture correction based on the accurately known point response function for the instrument. For sources identified as extended, isophotal magnitudes are used. IRAC data are expected to have a spatial resolution of $1''$–$2''$, sufficient that many SWIRE galaxies will be slightly extended. In the case of MIPS, the large *SIRTF* beam ($\approx 45''$ at 160 μm) ensures that all extragalactic targets will be point sources. Additionally, because of the large beam and *SIRTF*'s great sensitivity, nearly all of the MIPS data will suffer significantly from source confusion. In this case, point-source fitting is a more optimal extraction approach than aperture photometry, and so DAOPHOT and the SSC's APEX extraction software are under investigation.

Moving targets will be identified by multiepoch iteration of the SWIRE co-addition and source extraction pipeline. The data themselves are taken in multiple passes separated by a time period optimized for asteroid detection. A postprocessor will sort out all nonrepeating targets by location and then locate probable matches based on magnitudes and assumptions about target velocities. Lists will be compiled both of nonrepeating (transient) targets as well as moving targets.

The resulting lists of source fluxes and positions are then band-merged into catalogs that consist of a single source position and fluxes (or upper limits) in each of the *SIRTF* bands, based on source positions and their associated uncertainties, using the SSC pipeline band-merge module, which is based on that by the 2MASS project. For all sources in a given wavelength source list, a most likely counterpart is identified in adjacent wavelengths. Chains of associations are then generated and resolved. Band-merging of IRAC data is expected to be relatively straightforward because of the accurate *SIRTF* positions and the relatively small IRAC beam. Band-merging of MIPS data will be more problematic because these data suffer from a large beam size, resulting in significant source confusion, and also span a much larger range in wavelength and therefore a wider range in possible SEDs. The process is being optimized using extensive simulations with a wide range of known SED shapes. Initially, only the data taken with a given instrument will be band-merged, with band merging between the instruments to follow later. We are also investigating more sophisticated band-merging techniques based on the co-addition of multiwavelength images (e.g., Szalay, Connolly, & Szokoly 1999).

Details of this data processing, along with expected performance including an analysis of the completeness and reliability of extracted sources, will follow in an additional paper.

4.2. Data Products and Delivery Schedule

The SWIRE data will be archived and served to the community by the SSC, and the SWIRE ancillary data will be archived and served to the community by the IRSA at IPAC. Access to the two different data sets via these different archives will be seamless from the perspective of the user. In addition to the ancillary data described in § 2.3, the SWIRE/IRSA data archive will provide cross-links to data in the major large-area catalogs and data holdings, including 2MASS, *ROSAT*, SDSS, FIRST, NVSS, NED, and SIMBAD.

The *SIRTF* data products will include both processed images, subdivided into 0.5 deg^2 tiles, and source catalogs. Anticipated image data volumes range from 3.3 Gbytes for ELAIS N2 to 10.6 Gbytes for Lockman and ELAIS S1, including four images per tile: flux image, noise image, artifact map, and coverage map. The predicted catalog sizes range from about 130,000 sources in ELAIS N2 to as many 450,000 sources in Lockman and ELAIS S1. A prototype catalog data record is shown in Table 8 (subject to change).

Documentation describing the SWIRE data products will include an *Astrophysical Journal Supplement*–style paper describing the methods and results in full, metadata released with the data products, and archive help files for each catalog and each parameter.

The SWIRE data product delivery schedule is detailed in Table 9. The releases occur at semiannual intervals, beginning about 11 months after *SIRTF* launch. Successive deliveries will steadily expand the products with respect to increased area coverage, refinement of data-processing techniques, and improvement of the ensuing data products, decreasing signal-to-noise ratio (S/N) levels while maintaining high levels of completeness and reliability of the source extractions (completeness and reliability), validation to increasing levels of accuracy, and cross-matching to increasing numbers of bands and other catalogs.

5. PHOTOMETRIC REDSHIFTS AND SOURCE CHARACTERIZATION

SWIRE science goals depend strongly on accurate redshift estimates and source classification from our optical-IRAC-MIPS photometry. To complement *SIRTF* observations in the IR (3.6–160 μm), it is our goal to have optical (R/r'-band) observations for the whole sample; additional optical, near-IR, radio, and X-ray observations will be accessible for a subsample to allow detailed source characterization for representative populations.

5.1. Photometric Redshifts

By combining optical ground-based data with *SIRTF* data, we will be able to determine photometric redshifts for large samples of SWIRE sources, as well as to determine key parameters characterizing their infrared emission. The approach is based on the photometric codes of Rowan-Robinson (2003), which fit a set of six optical SED templates for normal galaxies, with the option to determine the extinction A_V. This code has been tested on available photometric catalogs in HDF-N and

TABLE 8
PROTOTYPE *SIRTF* CATALOG SOURCE ENTRY, MINIMUM COLUMN SET

Parameter	Number of Columns	Description
R.A., decl., and uncertainties	4	Final band-merged position
Flux (PSF-fit) and uncertainties, or limit	14	One per band
Flux (aperture) and uncertainties, or limit	14	One per band
S/N	7	One per band
Source reliability	7	One per band
Band-merge flags	6	One per neighboring band pair
Confusion flags	7	One per band
Cross-ID links	~10	One per catalog
Extent flag	7	One per band
Major axis	1	From multiband co-addition
Minor axis	1	From multiband co-addition
Position angle	1	From multiband co-addition
SED fit; best model SED	1	One per source
Photometric redshift and uncertainty	2	One per source
Coverage depth	7	One per band
Total	96	

HDF-S and gives robust estimates of redshift accurate to 10% in $1 + z$. The incidence of aliasing has been shown to be smaller than most other photometric redshift estimation codes. For application to *SIRTF* data, additional cirrus, starburst, and AGN dust torus components have been incorporated. An optical AGN accretion disk SED is also an option, and this is being tested against Sloan quasar catalogs.

The code has been run on prelaunch optical data prepared for SWIRE. Where four or more optical bands are available, redshifts are demonstrated to be reliable at the 98% level (i.e., no significant alias). Where only three optical bands are available, the reliability drops to 70%. Where UV data are available, an important by-product is the star formation rate in the galaxy. An optical SED type n_{typ} is also determined. Provided that at least four bands are available, an estimate of A_v is made. (An intercomparison of photometric redshift codes is being carried out by members of the SWIRE team and will be reported in a future publication.)

The majority of SWIRE galaxies are expected to be detected in the IRAC bands, especially the 3.6 and 4.5 μm bands. Since little contribution from dust emission is expected at the shorter IRAC wavelengths, IRAC photometry can be used to improve photometric redshift estimates for systems with multiband optical data. For systems with only R/r' imaging, approximate

TABLE 9
DATA RELEASE SCHEDULE

Date	Product
2003 Jul	V1.0 Sky simulations
2004 Jun	V1.0 Products: *SIRTF* image tiles and catalog; ancillary and preexisting images and catalogs; cross-IDs[a]
	V2.0 Sky simulations
2004 Dec	V1.0 Data analysis tools
	V1.0 Products: *SIRTF* image tiles and catalog; ancillary and preexisting images and catalogs; cross-IDs[b]
	V2.0 Products: *SIRTF* image tiles and catalog; ancillary and preexisting images and catalogs; cross-IDs[a]
2005 Jun	V3.0 Products: *SIRTF* image tiles and catalog; ancillary images and catalogs; cross-IDs
	V1.0 Band-merged catalog, IRAC-only and MIPS-only
2005 Dec	V4.0 Products: *SIRTF* image tiles and catalog; ancillary images and catalogs; cross-IDs
	V2.0 Band-merged catalog, including IRAC-MIPS
	V1.0 Lower S/N source release with validation analysis and flags
	V1.0 Moving object catalog, pending resources
	V1.0 Selection function (coverage maps convolved with final noise maps)
	V3.0 Sky simulations
2006 Dec	V5.0 Data products: final astrometry, band merging, confusion processing using cross-band information
	V5.0 XIDs between all V5.0 data products
	V4.0 Science simulations for fully developed science models

NOTE.—Release schedule subject to revision due to launch date or unanticipated on-orbit variances.

[a] SWIRE fields delivered to team by ~2004 January. Best efforts only on MIPS Ge.

[b] Remaining SWIRE fields.

photometric redshifts may be obtained from *R*-IRAC photometry alone. A bonus is that an estimate of the total stellar mass in the galaxy can then be made for galaxies with IRAC detection, at least at low redshifts. Where galaxies are detected at 4.5, 5.8, and 8 μm, an estimate can also be made of the luminosity in the cirrus component, after subtraction of the predicted stellar contribution. The ratio of L_{cirr} to, say, L_B should be related to the A_V value.

If there are also detections at 24 μm and beyond, estimates can be made of the luminosity in the starburst and AGN dust torus components. We describe the procedures we are further developing to address these questions in more detail in the next section. There are insufficient *SIRTF* bands for accurate photometric estimates of redshifts to be made from *SIRTF* data alone, given the presence of several components with distinct spectral signatures in the mid- and far-IR, and the large observed dispersion of dust temperatures found in ULIRGs (Blain, Barnard, & Chapman 2003; Farrah et al. 2003).

The above procedure has been prototyped against (1) *IRAS* galaxy samples and (2) simulated SWIRE data generated by C. K. Xu. The *IRAS* data are at different wavelengths from *SIRTF*, and the galaxies tend to be at low redshift (<0.3), but the code does successfully recover both the redshifts and the different SED components. The simulated data are, of course, highly dependent on the model assumptions, which are slightly different from those used in the deconvolution. The results of the simulations are again satisfactory.

In conclusion, depending on the number of detected bands, we expect to be able to output z, n_{typ}, $\dot{\phi}_*$, A_V, M_*, L_{cirr}, L_{sb}, and L_{tor} for large samples of SWIRE galaxies, which will be powerful diagnostics of galaxy evolution.

5.2. SEDs and Source Characterization

In addition to photometric redshift determination, we are developing methods to classify SWIRE sources based on the optical-radio SEDs in order to distinguish the main emitting components (starburst, AGNs) and the contribution of the stellar population. Our method is similar to the template-fitting technique applied to estimate photometric redshifts (Bolzonella, Miralles, & Pelló 2000). This method relies on the identification of spectral features strong enough to be preserved after the integration of the spectrum through the filter transmission curves. Emission lines can be useful if they are strong enough relative to the continuum flux to be detectable within broadband photometry. For objects with featureless spectra, the success of template fitting depends on the extent to which there exist unique continuum spectral shapes for source populations.

The far- (60–1000 μm), mid- (6–60 μm), and near- (1–6 μm) IR spectra of galaxies are characterized by different complexity and show distinct emitting components. The far-IR spectrum is featureless thermal radiation emitted by dust associated with an AGN, a starburst, or the galaxy disk, with temperatures ranging from a few tens to a few hundred kelvins. The mid-

IR spectrum is significantly more complex because of the variety of the emitting components: photodissociation regions (PDRs), H II regions (Tran 1998), and AGN-heated dust. Star-forming systems are dominated by the UIBs, which are produced in the PDRs at the interface between H II regions and molecular clouds. Very small grains associated with H II regions produce a more intense and steeper continuum at $\lambda > 12$ μm (Cesarsky et al. 1996; Verstraete et al. 1996; Roelfsema et al. 1996). The prominence of this component depends largely on the relative intensity of the UV radiation field of the galaxy. The spectrum of an AGN may show UIB features from star-forming regions or from the host galaxy disk (Mirabel et al. 1999; Clavel et al. 2000; Moorwood 1999; Alexander et al. 1999), but they are usually weaker than in starburst galaxies because of dilution from the strong continuum emitted by AGN-heated dust. The near-IR spectra of galaxies are dominated by stellar photospheric radiation. The stellar contribution can vary in galaxies with different star formation rates and stellar populations. The warm dust continuum is very faint at 7 μm (Cesarsky et al. 1996; Verstraete et al. 1996; Tran 1998) and is not generally detected in starbursts where the PDR emission (i.e., the UIB features) dominates (Sturm et al. 2000). Emission from AGN-heated dust can also contribute to flattening of the spectrum. If an AGN component or an extremely young ($\simeq 1$ Myr) stellar population does not dominate in the near-IR, a prominent feature at 1.6 μm appears in the near-IR spectrum of galaxies, caused by the minimum in the opacity of the H$^-$ ion present in the atmosphere of cool stars (John 1988).

In general, a starburst can be identified by strong PAHs, faint emission in the NIR, and cool MIR colors [$F(60$ μm$)/F(25$ μm$) > 5$] and an AGN by weak PAHs, strong NIR continuum, and warm MIR colors [$F(60$ μm$)/F(25$ μm$) \leq 5$]. However, the spectral differences between an AGN and a starburst are not always so distinctive. A significant continuum at short wavelengths (5–8 μm) is not necessarily a tracer of an AGN, but could reveal a higher emission from H II regions in the ISM than in PDRs (see, e.g., some dwarf metal-deficient starburst galaxies such as NGC 5253 and II Zw 40; Rigopoulou et al. 1999). Moreover, strong PAHs can also be observed in type II AGNs, where the hot dust continuum is absorbed by material along the line of sight (Clavel et al. 2000).

This variety of IR spectra makes any source characterization based on colors alone problematic. Our method is based on matching all observed data of SWIRE sources with templates representative of the known galaxy population. Existing template libraries derived from observed SEDs (Coleman, Wu, & Weedman 1980) or from models (Bruzual & Charlot 1993; Fioc & Rocca-Volmerange 1997; Leitherer et al. 1999; Silva et al. 1998; Devriendt, Guiderdoni, & Sadat 1999) either do not contain templates for AGNs, do not include dust emission, or do not extend behind NIR wavelengths. Regrouping the available models of a few galaxies obtained using different methods (Papovich & Bell 2002) produces a heterogeneous sample that

will not be representative of the full observed palette of IR spectra in SWIRE.

In order to create a complete, representative library of galaxy templates, we characterized the dispersion of galaxy IR spectra and then selected objects with well-sampled SEDs that could describe the observed variety of IR spectra. The optical-radio SEDs of 837 objects from the *IRAS* 25 μm sample (Xu et al. 2001) and the *ISO* PHT-S and PHT-L (Kessler et al. 1996) NIR SEDs of a sample of 175 normal and active galaxies (N. Lu 2002, private communication) were analyzed in order to select SEDs that span the full range of galaxy characteristics. The final catalog contains 37 SEDs with redshift from 0.0007 to 0.08 and two objects at redshift 1.06 and 1.44. In the optical and NIR, each SED was modeled using a spectrophotometric synthesis code (Berta et al. 2003; S. Berta et al. 2003, in preparation; J. Fritz et al. 2003, in preparation) derived from the spectral synthesis program by Poggianti, Bressan, & Franceschini (2001). In the MIR, we adopted the observed spectrum between 2.4 and 11 μm observed with *ISO* PHT-S and PHT-L and the SEDs as modeled by Xu et al. (2001) at longer wavelengths. Templates for quasars were derived by combining composite optical spectra from the FIRST Bright Quasar Survey[30] (Brotherton et al. 2001) and the observed spectrum of a red quasar (Gregg et al. 2002) with *ISO* PHT-S and PHT-L NIR SEDs and photometric data in the IR of quasars with optical SEDs well fitted by the composite spectra. The library contains templates for ellipticals, spirals, irregulars, starburst, ULIRGs, and active galaxies covering the wavelength range between 300 Å and 20 cm. All the current templates are shown in Figure 7.

The completeness of the current library is being tested using multicolor photometric catalogs of galaxies at low and high redshifts with different sets of filters and selection effects, such as the catalogs of the HDF-N (Fernández-Soto et al. 2001) and of CDF-S (Barger et al. 2002), the quasars observed with *ISO* (Polletta et al. 2000; Haas et al. 2000; Andreani et al. 2003; Kuraszkiewicz et al. 2003), the CfA Seyfert sample (Pérez García & Rodríguez Espinosa 2001), ULIRG samples (Klaas et al. 2001; Farrah et al. 2003), and the *IRAS* 25 μm sample (Shupe et al. 1998; Xu et al. 2001). New templates will be added to represent observed SEDs that are not fitted by the current templates. Our library contains mostly SED of local galaxies and only two high-z objects. Distant galaxies likely differ from local galaxies in their IR SEDs (Xu et al. 2001; Dole et al. 2003), and therefore new templates may be added to the existing library to represent the high-redshift galaxy population when more knowledge about this population is available.

The bulk of SWIRE sources will be detected only at shorter wavelengths (IRAC). Thus, full coverage of galaxies' IR SEDs with accurate photometry may be possible for only relatively nearby or bright objects. Therefore, the limitations of our
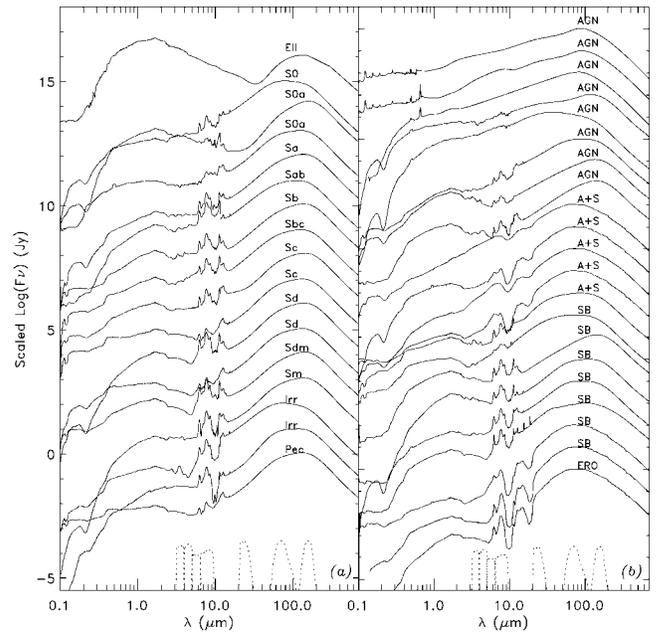

FIG. 7.—Galaxy templates for (*a*) normal galaxies and (*b*) starburst, AGNs, and ULIRGs. The IRAC and MIPS filter transmission curves are shown as dotted curves.

method are being investigated on simulated catalogs with solely IRAC data or IRAC plus one optical band. In particular, the degeneracy between redshift, dust temperature, age, and extinction is under study.

Our galaxy template library provides a tool to investigate which colors can be used to distinguish different types of objects. Sawicki (2002) claims that *SIRTF* NIR data alone should be sufficient to identify most galaxies at $z \geq 1.5$ that are dominated by stellar populations older than ≥ 20 Myr through the 1.6 μm bump. Galaxies at lower redshifts or those dominated by very young stellar populations suffer from severe degeneracies, and their SEDs can be fitted if either IR observations at shorter wavelengths or optical data are included. The color analysis cannot provide an accurate source classification for the entire SWIRE sample because of the degeneracies among different objects. However, some objects have unique colors and can be easily identified: (1) ULIRGs can often be identified through the 70/8 μm ratio, (2) type I AGNs with $0.1 \leq z \leq 1.6$ using the IRAC 5.8 μm/IRAC 3.6 μm ratio, and (3) and objects such as Mrk 231, a type I AGN and ULIRG using the blueness of the IRAC or optical-IRAC colors. The FIR color $F(70 \mu$m$)/F(160 \mu$m$)$ can provide estimates of the FIR luminosity (L_{FIR}), depending on how well the correlation observed for local galaxies holds for galaxies up to redshift 3 (Chapman et al. 2002; Blain et al. 2003). The optical/IR flux ratio may also work well as a luminosity estimator (see Fig. 10*b*).

Additional tools to characterize SWIRE sources will be provided by the morphological analysis in optical images and by

---

X-ray data. Optical imaging will provide morphological information about the objects that can be used to distinguish spheroids from disk galaxies and identify mergers. X-ray emission is a good tracer of AGNs, even if star-forming galaxies can also emit X-rays through X-ray binaries, supernovae, and hot diffuse gas. However, the X-ray emission of starburst galaxies is fainter and softer than the AGN X-ray emission.

The final library of galaxy templates with data and spectral models, the method for SWIRE source classification, and the tests on existing photometric catalogs will be published in a separate paper.

6. EARLY SCIENCE WITH SWIRE

Since SWIRE is a homogenous, multiwavelength survey covering a large area of sky and producing several million sources, the science possibilities with it are enormous. In this section, we very briefly outline the main science topics that the SWIRE team plans to address initially.

6.1. Modes and Rates of Star Formation

As described in § 1, a fundamental question for galaxy evolution is the relative importance of quiescent star formation versus starbursts as a function of epoch and matter density/environment. SWIRE will directly measure the mid- to far-IR SEDs of ~100,000 IR-luminous galaxies. The expected SWIRE source detection statistics are summarized in Figure 8, which shows results for two contrasting phenomenological models from Xu et al. (2003) and Rowan-Robinson (2001) (see § 3.1). Model S3 of Xu et al. (2003) is dominated by starbursts at high redshift, while Rowan-Robinson (2001) attributes more sources to cooler, disk-dominated galaxies.

The 70 μm band will sample the broad peak of typical dust temperature components (~35 K) out to redshifts of about 0.5 and warmer ones (~70 K) to redshifts about 1, while the less sensitive 160 μm band can sample the most luminous sources in these temperature ranges to redshifts above 1 and 3, respectively. Over these redshift and temperature ranges, the SWIRE multiwavelength SEDs will provide an accurate measurement of the bolometric luminosity of the galaxy and the dust temperature range present. Using photometric redshifts (see § 5.1) derived from the optical/IRAC data, we will construct luminosity functions in many separate volume cells and for different dust temperature ranges. Prior to the availability of photometric redshifts, the same questions can be addressed to lesser accuracy using number/color/flux data, e.g., Figures 9 and 10.

Many systems will be detectable in the 8 and 24 μm bands to redshifts $z \sim 3$ or higher, although SWIRE will not sample their IR SEDs at peak and so will not directly determine their IR luminosities.

A primary goal of SWIRE is to determine the cause for the strong increase in the global star formation rate between $z \sim 0$ and $z \sim 1$ as measured by the IR energy density. SWIRE will focus on the nature of the most luminous sources, which seem to be much more numerous at high redshift and which provide the most critical challenges to hierarchical models in terms of the extreme star formation rates required at high redshift. We will address this by finding these systems (with MIPS), studying their old stellar populations (with IRAC), observing their morphologies (with the optical imaging), and determining their environments (all data). We can investigate the relative importance of quiescent star formation versus starbursts from 160/70 μm colors (Fig. 9) and morphology, looking, for example, for large disks rather than the major mergers that dominate local ULIRGs. Quiescent, distributed star formation occurring over galaxy disks should be cooler than nuclear starbursts; thus we can directly track these modes and test models that attribute the high fluxes of high-redshift *ISO* 170 μm and submillimeter sources to distributed "cirrus" emission (Rowan-Robinson 2001; Efstathiou & Rowan-Robinson 2003; Xu et al. 2003; Kaviani et al. 2003), e.g., compare the models of Xu et al. (2003) and Rowan-Robinson (2001) in Figure 8, and Xu et al. (2003) model S2 in Figure 9.

In Figure 10 (*left panel*), we show the anticipated color distribution in the 70/24 versus 1.4 GHz/70 μm color-color plane for model S3 for our deep VLA field (§ 2.3.5). In this model, ~90% of the SWIRE MIPS population is detected at 20 cm, which will allow an interesting investigation of the radio/IR correlation at high redshifts (the model assumes no ratio evolution). Note that the very large dispersion in observed 1.4 GHz/70 μm color is dominated by the dispersion in redshift but also incorporates the intrinsic dispersion in the template SEDs (see Xu et al. 2003 for full details). It remains to be seen whether the local radio/IR correlation holds up at high redshifts.

Figure 10 (*right panel*) shows the well-known infrared/optical flux density ratio versus L_{ir} relation from the local universe (Soifer et al. 1989). The apparent horizontal tracks in this figure are due to individual template SEDs, which are fixed in luminosity, sampled by the model galaxy population over a range of redshifts. While this "k-correction" dispersion degrades the use of this relation as a luminosity indicator at higher luminosities, we can use it to estimate minimum luminosities and hence a lower limit to luminosity distance using the measured flux. This technique of course assumes that the high-redshift SEDs have been well represented by the model, which may not turn out to be the case.

6.2. The Mass Function of Spheroids

SWIRE will detect ~1 million spheroids by the emission of evolved stars in the shorter IRAC bands, reaching $z \sim 2.5$ (Fig. 8). The stellar mass of these systems can be estimated by SED fitting using a library of stellar population synthesis models (e.g., Dickinson et al. 2003). This method has been prototyped for SWIRE using the models of Poggianti et al. (2001) by Franceschini et al. (2003), who found fairly large uncertainties in estimated stellar masses for *ISO*-detected HDF galaxies when using only optical/NIR data, especially if a there
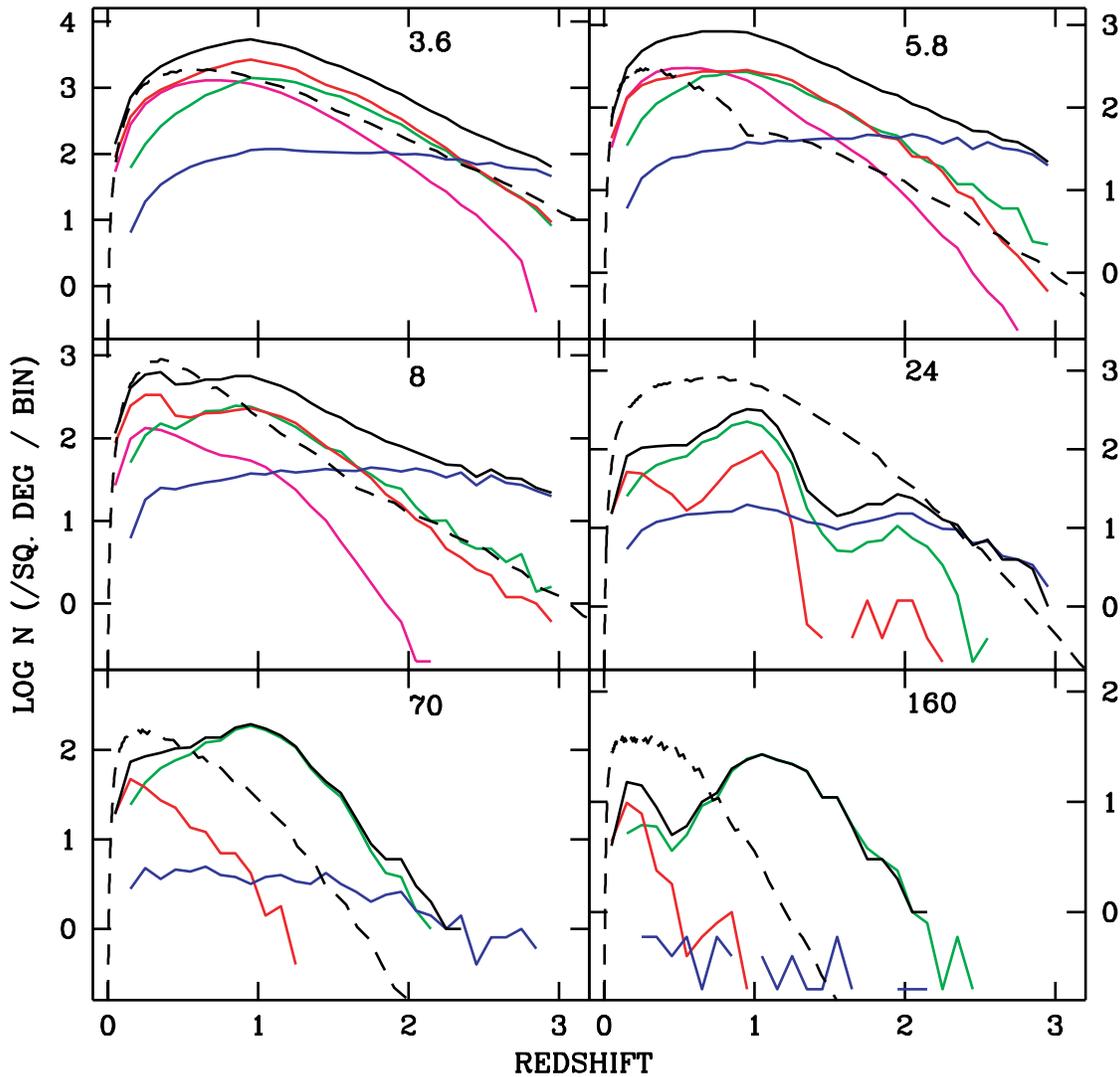
FIG. 8.—Redshift distributions per 0.1 redshift bin per square degree in six SWIRE *SIRTF* bands. The models depicted are S3 and E2 of Xu et al. (2003; *solid lines*) and Rowan-Robinson (2001; *dashed line*). The flux limits are the 5 σ sensitivity limits from Table 3, except where confusion noise is expected to dominate, namely, $S_{\text{lim}}(70\ \mu\text{m}) \sim 6$ mJy, $S_{\text{lim}}(160\ \mu\text{m}) \sim 60$ mJy. For the Xu et al. (2003) models, the contribution of each galaxy type is indicated by color: spheroids (*magenta*), disks (*red*), starbursts (*green*), AGNs (*blue*), and total (*black*).

exists a substantial stellar population with significant extinction. The addition of photometry in the IRAC bands will provide much greater accuracy because older populations dominate these longer wavelength bands, rendering the SEDs very uniform (Simpson & Eisenhardt 1999; Sawicki 2002). The longer wavelength IRAC bands also enable robust mass estimation over a much larger redshift window.

Using the SWIRE $r' - 5\ \mu\text{m}$ SEDs, we will assess the build-up rate of stellar mass in massive stellar systems since $z \sim 2.5$ and compare it directly to the global star formation rates in IR-luminous systems, for both quiescent and starburst modes, over the same redshift range. Again, the dependence of the results on the matter density field and the nearby galaxy environment

will be of primary importance to constraining galaxy formation models and the cosmological model.

6.3. Active Galactic Nuclei

As described in § 1, a major SWIRE goal is to determine the evolving number density of AGNs, particularly heavily obscured ones. The difficult aspect of this goal lies in identifying the AGNs, because the most heavily obscured ones can be very optically thick even in the near- and mid-IR, where we expect the unique AGN identification signatures, specifically warm dust associated with the torus in the $3\ \mu\text{m} < \lambda <$
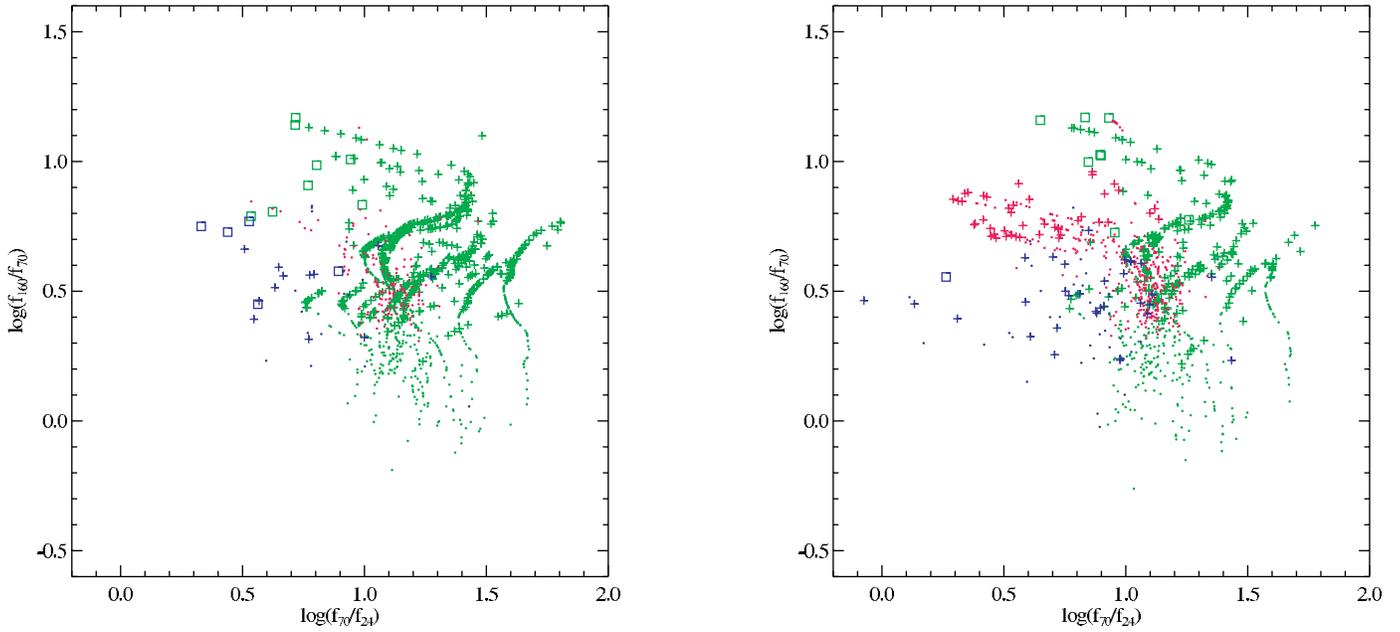
FIG. 9.—SWIRE dusty populations within 1 deg² for model S3 (*left panel*) and model S2 (*right panel*). Disks are red, starbursts are green, and AGNs are blue. Symbols denote redshift range: $z < 1$ (*dots*), $1 < z < 2$ (*pluses*), $z > 2$ (*squares*).
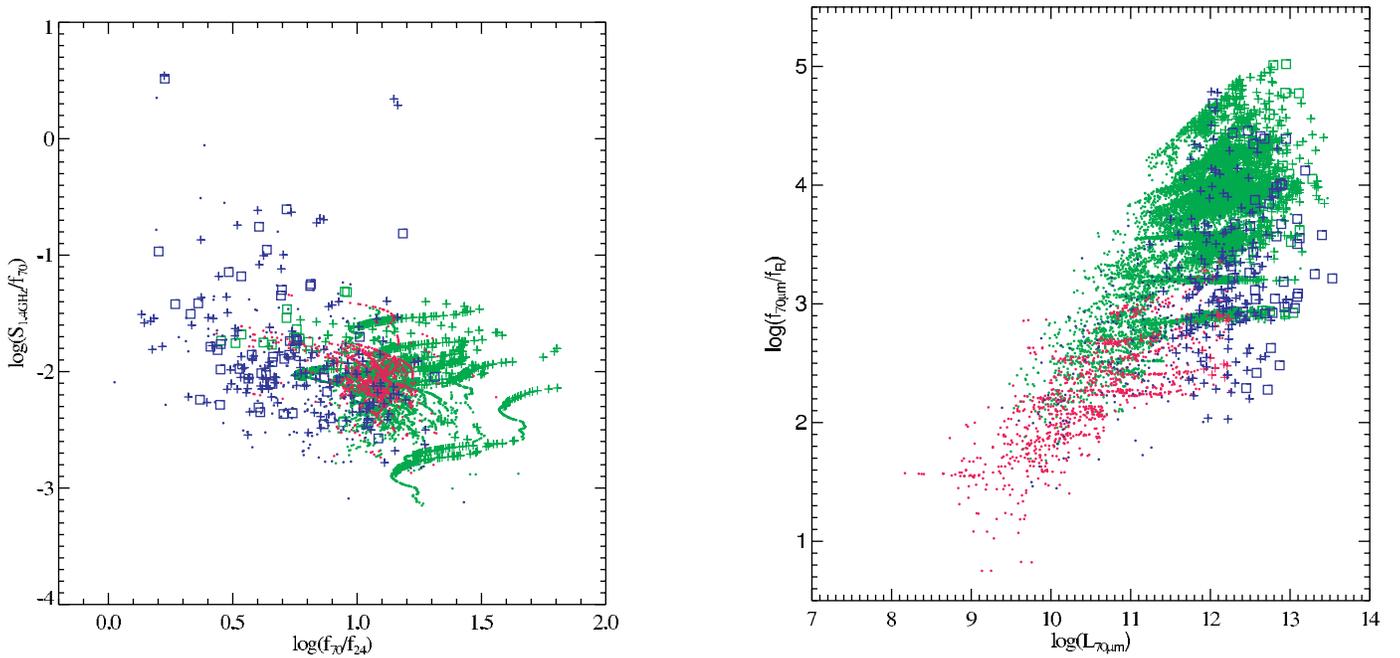

FIG. 10.—*Left panel:* MIPS/20 cm color-color plot for the same population described in Fig. 9. The radio flux density limit is 16 μJy, corresponding to ~5 σ in our ultradeep VLA image. *Right panel:* 70 μm/R color vs. $L_{70 \mu m}$.

40 μm range, and very red colors due to extinction in the near-IR, such as are being found for moderately obscured 2MASS AGNs (Lacy et al. 2001; Cutri 2001). Our initial studies of SWIRE AGN populations will be based on identifying candidates with indicators of heavy extinction from red optical-IRAC colors and warm dust from 3–70 μm colors.

The blue curves in Figure 8 illustrate the detectabilty of *optically selected* AGNs by SWIRE. If obscured populations such as those required to explain the slope of the XRB increase with redshifts and are actually more numerous than low-obscuration AGNs by factors of up to 4, as observed in the deep *Chandra* surveys (Gilli 2002), then a substantial fraction of the SWIRE "starburst" sources (*green curves*) will harbor such AGNs. Moreover, these AGNs may possibly warm the MIPS colors above those assumed in our models, which would boost the relative 24 and 8 μm counts still further.

Statistical studies of the starburst/AGN connection as a function of luminosity will provide major insights into how starbursts and AGNs coexist and to possible evolutionary relationships. Furthermore, we can examine starburst-AGN connections as a function of redshift (thus increasing gas mass, decreasing dust content, and decreasing metallicity), environment, and Hubble type.

6.4. Large-Scale Structure

Our first large-scale structure goal will be to provide an estimate of the clustering of both active and passive galaxies with mean redshifts higher than any substantial surveys to date, using two-dimensional autocorrelation functions. Such measurements are expected to provide powerful constraints on models of galaxy formation.

We will measure the angular autocorrelation functions of the SWIRE galaxies selected in each of the seven *SIRTF* bands, comparing each of these seven autocorrelation functions with predictions from existing numerical and semianalytic models of galaxy formation and with extrapolations from existing surveys at other wavelengths and lower redshifts. Inversion techniques will provide an estimate of three-dimensional clustering, against which future models can be directly compared. This will require model redshift distributions or real redshift distributions as they become available.

Other two-dimensional two-point statistics including the power spectrum and variance of counts in cells may also be investigated.

Two-dimensional cross-correlations can provide a better handle on the issue of galaxy bias, by allowing us to investigate the relative clustering of different subsamples of the SWIRE populations. We will measure the angular cross-correlation between galaxy catalogs selected at different *SIRTF* wavelengths. Initially we will focus on comparing the IRAC and MIPS catalogs, as these probe passive and active star formation systems, respectively. As our classification of galaxies on the basis of their multiwavelength colors improves, we will compare distinct populations, e.g., starburst galaxies, spheroids, and AGNs. Measurements of cross-clustering statistics will be compared with predictions from existing models, and inversion techniques will provide estimates of three-dimensional cross-clustering.

Once we have established a reasonable photometric redshift system, we will be able to provide an estimation of the evolution of the clustering, independently of other low-redshift surveys, by repeating the above analyses in photometric redshift slices. We can also use these photometric redshifts to provide better estimates of three-dimensional clustering without resorting to inversion techniques.

As a more subtle test of galaxy formation models, we also intend to use counts-in-cells techniques to investigate the higher order statistics of galaxy clustering. We will perform two-dimensional counts-in-cells analyses on individual populations and on joint populations. We will also use photometric redshifts to take these analyses into three dimensions.

Ultimately, in collaboration with the wider astronomical community, we hope to obtain sparse redshift surveys to provide a better precision and check on our photometric redshift-based studies.

6.5. Clusters in the *XMM*-LSS Field

A major goal for the *XMM*-LSS field is comparative cluster detection in terms of galaxy and cluster properties. In parallel to optical multicolor and X-ray cluster detection techniques, we shall investigate clustering methods in the *SIRTF* wave bands; this is a totally new approach with the potential to yield distant clusters of AGNs as well. Clusters will principally be detected by late-type stellar emission of individual cluster members in the shortest IRAC bands, but at the higher redshifts star formation and AGN activity is expected to increase, detectable by dust emission in the longer *SIRTF* bands. We will compare cluster existence/richness/morphology derived in the different wave bands. Although these techniques provide comparable results in the local universe, there are strong hints that the overlap between optically and X-ray–selected clusters beyond $z > 0.5$ is only ~60% (Donahue et al. 2001, 2002). It is most interesting to understand this discrepancy. One possibility is that optical cluster selection is very sensitive to the star formation rate owing to the effect on galaxy color by active star formation.

A further goal is to determine the location of the SWIRE sources within the cosmic network. Environmental studies of the *XMM*-LSS data (X-ray and optical) will provide a unique view of the LSS out to $z \sim 1$. Redshift measurements of the SWIRE sources will allow us to subsequently locate them within the cosmic network (field, filaments, groups, clusters). This will provide decisive clues as to the effect of environment on star, galaxy, and AGN formation. Ultimately, one can relate environmental conditions to the initial density fluctuations from which the clusters originated. Conversely, we shall be in a

position to investigate how galaxy activity affects the global properties of clusters such as metallicity, temperature, etc., and thus quantitatively address such questions as the effect of pre-heating by star formation and AGNs on the intracluster medium. Another point will be to investigate whether star formation and nuclear activity are, as expected, most efficient in medium dense environments (i.e., groups), since in these regions, galaxy velocities are moderate, thus optimal for efficient interactions.

A third study will use clusters as gravitational telescopes to flag and study very distant SWIRE sources. Weak lensing studies using the Canada-France-Hawaii Legacy Survey data on the most massive X-ray–detected clusters will offer a truly new window to the distant universe, and we expect as well several SWIRE sources per cluster to be the magnified images of very distant (obscured?) objects. We shall thus gather a sample of several tens of pencil-beam surveys, providing a statistical complement to the study undertaken by GOODS and, in addition, less affected by possible instrumental confusion effects.

6.6. Mergers, Environment, and Morphological Evolution

SWIRE will provide a unique window into the development of the Hubble sequence by providing true AGN and starburst luminosities associated with merger-driven events and other environmental factors such as cluster-cluster mergers, over large comoving size scales at $z \sim 1–2$. Moreover, the depth and angular resolution (particularly at IRAC wavelengths) of the *SIRTF* observations will be very high for local objects. For these we can address the detailed structural relationships between the optical/near-IR/submillimeter structure and the mid-IR structure in a wide variety of galaxies.

A few of the planned follow-up projects for the SWIRE data include pointed high-resolution optical imaging of ULIRGs at medium and high redshift, adaptive-optics surveys of galaxies lying in the SWIRE fields, a study of optically identified interacting galaxies using the SWIRE optical and infrared data, a high-resolution submillimeter study of SWIRE interacting, infrared luminous galaxies, optical asymmetries in UV versus IR-selected galaxies, the star formation rate as a function of environmental richness, and an unbiased high spatial resolution optical survey of a large fraction of a SWIRE field.

6.7. Rare Objects

A major strength of SWIRE is the large cosmological volume available to it; therefore, the sample will contain unusual objects of up to 1 in 10^6 rarity, to redshifts greater than 3. These will include both object types we already know about such as extremely red objects (EROs), Lyman break galaxies (LBGs), distant ULIRGs such as discovered by SCUBA, powerful QSOs and radio galaxies, and brown dwarfs. We may also anticipate previously unknown categories of objects that

SWIRE may select in favor of, such as galaxies with unusually warm mid-IR colors. The individual objects will be extremely interesting in their own right and also as elements in the major science themes discussed in previous sections. For example, very distant and luminous ULIRGs and AGNs detected at 8 and/or 24 μm will be used as potential tracers of massive halos. A major goal is to measure the mid- and far-IR luminosity distributions of LBG candidates (Siana et al. 2002).

Rare object candidates will be selected by their flux-color signatures in the multiwavelength SWIRE databases and followed up extensively, both on the ground and with *SIRTF* deeper imaging and IRS spectroscopy (beginning with a small GTO IRS program to follow up around six SWIRE sources in Lockman; PI: M. Werner).

6.8. Nearby Galaxies

The large area of the SWIRE survey, together with *SIRTF*'s higher sensitivity and better angular resolution than previous IR space telescopes, allows us and the community to undertake a number of investigations of galaxies in the local universe. Galaxies with diameters larger than $\sim 10''$ will be spatially resolved by *SIRTF* in the IRAC bands and those larger than $\sim 15''$ also in the 24 μm MIPS band. The largest of the nearby galaxies present in the survey area could also be resolved at 70 and 160 μm. The *SIRTF* Legacy project *SIRTF* Nearby Galaxy Survey (SINGS; Kennicutt et al. 2003) is designed to study the physics of the star-forming ISM and galaxy evolution by a comprehensive imaging and spectroscopic study of 75 nearby galaxies ($D < 30$ Mpc). SWIRE will extend some of these investigations to a larger sample of galaxies at larger redshifts and in very different galaxy environments, including isolated galaxies, interacting galaxies, groups, and clusters.

We have defined a prototype SWIRE nearby galaxy sample from the 2MASS final reduced database, searching in the SWIRE areas for objects with isophotal diameter at 2.2 μm (the 2MASS band closest in wavelength to the IRAC spectral range) greater than $10''$. The sample consists of several hundred galaxies with angular diameters up to $\sim 100''$. A small number of galaxies are contained in the 2MASS Large Galaxy Atlas (Jarrett et al. 2003). One of the largest is NGC 5777 in the Lonsdale field, which is illustrated in Figure 11. Most of the galaxies with a published redshift are at $z < 0.1$.

The *SIRTF* broadband images, combined with data at other wavelengths (e.g., UV imaging from the *Galaxy Evolution Explorer*), will allow us to study in detail the physics of star formation as a function of location in the galaxy, ISM properties, galaxy morphological and spectral type, and galaxy environment, particularly for objects of relatively low IR luminosities, which will not be detectable at higher redshift. The sample will also be used to construct composite SEDs for different galaxy types, which will be useful to interpret the SEDs of more distant objects.
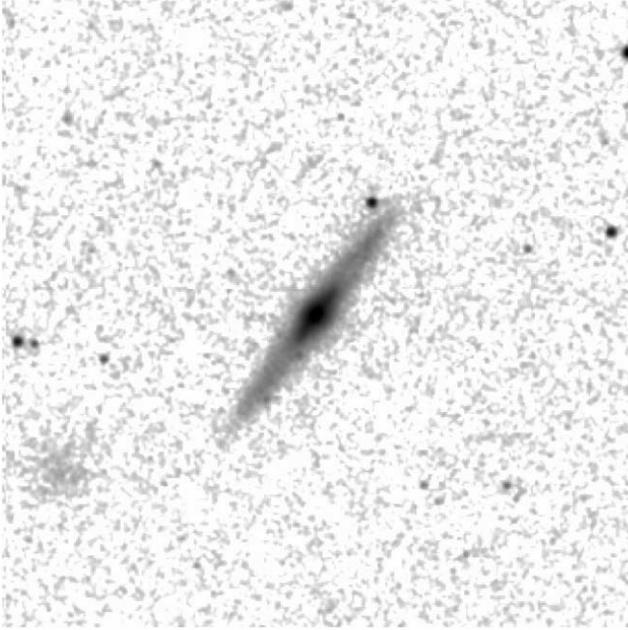
Fig. 11.—NGC 5777 as seen in the combined 2MASS near-infrared bands. The 1 σ surface brightness is 21.8 mag arcsec^{-2}, and the resolution is ~3″. To the lower left (southeast) of the image center is the dwarf companion UGC 09570. The image size is 5′.7 on a side.

6.9. Brown Dwarfs

During the past few years, a large number of very low mass stars and substellar objects ("L" dwarfs) have been discovered, primarily in the near-infrared 2MASS and DENIS surveys (Oppenheimer, Kulkarni, & Stauffer 2000) and more recently in the SDSS (Geballe et al. 2002). These objects lie below the M dwarfs in effective temperature and are primarily distinguished by their very red *JHK* colors. However, even cooler objects, designated "methane" or "T dwarfs" (Burgasser et al. 2002), are more difficult to find in these near-IR surveys, since their methane bands give them a blue color shared by many ordinary disk stars. The IRAC 3.6/4.5 μm bands are ideal for identification of T dwarfs. The 3.6 μm channel encompasses a major methane band, while the 4.5 μm channel samples the SED peak for these cool sources. Thus, the $F_{4.5} - F_{3.6}$ color should easily pick out nearby T dwarf candidates in our source list. SWIRE will provide the best *SIRTF* Legacy database for serendipitous brown dwarf discoveries because of its wide area coverage and high sensitivity. SWIRE will have sufficient 4.5 μm sensitivity and areal coverage to potentially detect very low mass old brown dwarfs in the field. Comparing the SWIRE sensitivities (Table 3) to the predicted fluxes for old BDs from Burrows et al. (1997), we find that SWIRE could detect a 5 Gyr old, 275 K brown dwarf at a distance of 10 pc at 4.5 μm.

We simulated the detectability of field brown dwarfs in the

SWIRE legacy survey using a Monte Carlo model similar to Martín et al. (2001), who estimated brown dwarf number counts for a range of IRAC survey sizes and sensitivities. Fluxes in the four IRAC bandpasses were tabulated versus effective temperatures using the online models of Marley; T_{eff} versus mass and age was taken from evolutionary models by A. Burrows. Brown dwarf initial mass functions with various power law indices α were simulated, with total counts normalized to the adopted stellar space density of 0.057 pc^{-3} (Reid et al. 1999). A star formation rate proportional to $1 - \exp\left(-t/\tau_1\right)\exp\left(-t/\tau_2\right)$ was used, with $\tau_1 = 0.2$ and $\tau_2 = 8.0$ Gyr. Random masses, ages, and *X*, *Y*, *Z* coordinates within a Sun-centered cubical volume were then used as inputs to the evolution and mid-IR flux models, which were interpolated to give the observables. For $\alpha = 1.5$, 1.0, and 0.5, the model predicts SWIRE detection of 23, eight, and one objects, respectively, in IRAC channel 2 (4.5 μm).

6.10. Circumstellar Debris Disks

Among the most important questions in astronomy today are the frequency of extrasolar planetary systems and their similarity to our own solar system. *SIRTF*'s extremely high sensitivity at long wavelengths enables investigation of circumstellar disks that are plausible signposts of debris from planet formation. Disks similar to the one observed around HR 4796A (Koerner et al. 1998) show excess emission from dust at wavelengths beyond 8 μm with a steep rise between 24 and 70 μm, ideal for study with MIPS. *IRAS* detected debris disks around massive stars at distances of tens of parsecs. *SIRTF* will be able to detect much more tenuous disks around solar-type stars out to 100 pc and analogs of HR 4796A (A0 star) at a kiloparsec. Even considering the high Galactic latitudes of our survey fields, we expect to detect the photospheres of at least 1000 A–K spectral type stars at 24 μm. The frequency of dust excess among stars in the solar neighborhood is at least 15% (Lagrange, Backman, & Artymowicz 2000), so we would plausibly expect to discover on the order of 150 new debris disk systems during our MIPS surveys. Unlike the other *SIRTF* Legacy debris disk searches, SWIRE will have no age or spectral type bias in its survey of debris disks.

6.11. Small Asteroids

Current knowledge of the asteroid size-frequency distribution is limited to sizes larger than about 10 km. The population of small asteroids is almost completely uncharacterized but is critical for understanding the parent population of the Earth-crossing asteroids (Evans et al. 1998). *SIRTF* will be sensitive to thermal emission at 8 and 24 μm from main-belt asteroids as small as 1 km. Estimates of the number of asteroids in *SIRTF* 5′ × 5′ images at ecliptic latitude 0° range over at least an order of magnitude. Although most of our survey fields are

located at high ecliptic latitude, the *XMM*-LSS (9 deg^2) field is at 17° latitude. We will repeat the MIPS scans across this field at an interval of several hours, allowing us to identify asteroids and to estimate their mean motion.

REFERENCES

Alexander, D. M., Efstathiou, A., Hough, J. H., Aitken, D. K., Lutz, D., Roche, P. F., & Sturm, E. 1999, MNRAS, 310, 78
———. 2001, ApJ, 554, 18
Almaini, O., et al. 2003, MNRAS, 338, 303
Andreani, P., Cristiani, S., Grazian, A., LaFranca, F., & Goldschmidt, P. 2003, AJ, 125, 444
Archibald, E., Dunlop, J., Jiminez, R., Friaca, A., McClure, R., Hughes, D. 2002, MNRAS, 336, 353
Ashby, M., Surace, J., & Hora, J. 2003, Proc. SPIE, 4850, 50
Babul, A., & Postman, M. 1990, ApJ, 359, 280
Barger, A. J., Cowie, L. L., Brandt, W. N., Capak, P., Garmire, G. P., Hornschemeier, A. E., Steffen, A. T., & Wehner, E. H. 2002, AJ, 124, 1839
Beichman, C. A., Cutri, R., Jarrett, T. J., Steining, R., & Skrutskie, M. 2003, ApJ, in press
Benson, A. J., Frenk C. S., Baugh C. M., Cole S., & Lacey C. G. 2001, MNRAS, 327, 1041
Berta, S., Fritz, J., Franceschini, A., & Bressan, A. 2003, A&A, submitted
Bertin, E., & Arnouts, S. 1996, A&AS, 117, 393
Blain, A. W., Barnard, V. E., & Chapman, S. C. 2003, MNRAS, 338, 733
Blain, A. W., Jameson, A., Smail, I., Longair, M. S., Kneib, J.-P., & Ivison, R. J. 1999, MNRAS, 309, 715
Blain, A. W., Smail, I., Ivison, R. I., Kneib, J.-P., & Frayer, D. T. 2002, Phys. Rep., 369, 111
Blanton, M., Cen, R., Ostriker, J. P., Strauss, M. A., & Tegmark, M. 2000, ApJ, 531, 1
Bolzonella, M., Miralles, J.-M., & Pelló, R. 2000, A&A, 363, 476
Brotherton, M., Tran, H., Gregg, M., Becker, R., Laurent-Meuhleisen, S., & White, R. 2001, ApJ, 546, 775
Bruzual, G. A., & Charlot, S. 1993, ApJ, 405, 538
Burgasser, A., et al. 2002, ApJ, 564, 421
Burrows, A., et al. 1997, ApJ, 491, 856
Cambresy, L., Beichman, C., Jarrett, T., & Cutri, R. M. 2002, AJ, 123, 2559
Cesarsky, D., Lequeux, J., Abergel, A., Perault, M., Palazzi, E., Madden, S., & Tran, D. 1996, A&A, 315, L309
Chapman, S. C., Blain, A., Ivison, R. J., & Smail, I. 2003, Nature, 422, 695
Chapman, S. C., Smail, I., Ivison, R. J., Helou, G., Dale, D. A., & Lagache, G. 2002, ApJ, 588, 186
Chary, R., & Elbaz D. 2001, ApJ, 556, 562

Ciliegi, P., Zamorani, G., Hasinger, G., Lehmann, I, Szokoly, G., & Wilson, G. 2003, A&A, 398, 901
Clavel, J., et al. 2000, A&A, 357, 839
Cohen, A. S., et al. 2003, ApJ, 591, 640
Cole, S., Lacey, C. Baugh, C., & Frenk, C. 2000, MNRAS, 319, 168
Coleman, G. D., Wu, C.-C., & Weedman, D. W. 1980, ApJS, 43, 393
Colless, M., et al. 2001, MNRAS, 328, 1039
Comastri, A., Fiore, F., Vignali, C., Matt, G., Perola, G., & La Franca, F. 2001, MNRAS, 327, 781
Condon, J. J., et al. 1998, in Observational Cosmology with the New Radio Surveys, ed. M. N. Bremer, N. Jackson, & I. Pérez-Fournon (Dordrecht: Kluwer), 37
Conselice, C. 2003, in Galaxy Dynamics, ed. C. Boily, P. Patsis, C. Theis, S. Portegies Zwart, & R. Spurzem (Paris: EDP Sciences), in press (astro-ph/0212468)
Cutri, R. 2001, in IAU Colloq. 184, AGN Surveys, ed. R. Green, E. Kachikian, & D. Sanders (ASP Conf. Ser. 284; San Francisco: ASP), 5
Dekel, A. 1994, ARA&A, 32, 371
de Ruiter, H. R., et al. 1997, A&A, 319, 7
Devriendt, J. E. G., & Guiderdoni, B. 2000, A&A, 363, 851
Devriendt, J. E. G., Guiderdoni, B., & Sadat, R. 1999, A&A, 350, 381
Dickinson, M., Papovich, C., Ferguson, H., & Budavari, T. 2003, ApJ, 587, 25
Dole, H., Lagache, G., & Puget, J.-L. 2003, ApJ, 585, 617
Dole, H., et al. 2001, A&A, 372, 364
Donahue, M., et al. 2001, ApJ, 552, L93
———. 2002, ApJ, 569, 689
Efstathiou, A., & Rowan-Robinson, M. 2003, MNRAS, 343, 322
Efstathiou, G., Kaiser, N., Saunders, W., Lawrence, A., Rowan-Robinson, M., Ellis, R. S., & Frenk, C. S. 1990, MNRAS, 247, 10P
Elbaz, D., et al. 1999, A&A, 351, L37
Ellis, R. S., Smail, I., Dressler, A., Couch, W. J., Oemler, A., Jr., Butcher, H., & Sharples, R. M. 1997, ApJ, 483, 582
Evans, R. W., et al. 1998, Icarus, 131, 261
Fadda, D., Flores, H., Hasinger, G., Franceschini, A., Altieri, B., Cesarsky, C. J., Elbaz, D., & Ferrando, Ph. 2002, A&A, 383, 838
Fan, X., et al. 2003, AJ, 125, 1649
Fardal, M. A., Katz, N., Gardner, J., Hernquist, L., Weinberg, D., & Dave, R. 2001, ApJ, 562, 605

Farrah, D., Afonso, J., Efstathiou A., Rowan-Robinson, M., Fox, M., & Clements, D. 2003, MNRAS, in press (astro-ph/0304154)

Farrah, D., Serjeant, S., Efstathiou, A., Rowan-Robinson, M., & Verma, A. 2002a, MNRAS, 335, 1163

Farrah, D., Verma, A., Oliver, S., Rowan-Robinson, M., & McMahon, R. 2002b, MNRAS, 329, 605

Farrah, D., et al. 2001, MNRAS, 326, 1333

Fazio, G., et al. 2003, *SIRTF* Guaranteed Time Observation Program

Fernández-Soto, A., Lanzetta, K., Chen, H.-W., Pascarelle, S., & Yahata, N. 2001, ApJS, 135, 41

Fioc, M., & Rocca-Volmerange, B. 1997, A&A, 326, 950

Fox, M. J., et al. 2002, MNRAS, 331, 839

Franceschini, A., Aussel, H., Cesarsky, C. J., Elbaz, D., & Fadda, D. 2001, A&A, 378, 1

Franceschini, A., Braito, V., & Fadda, D. 2002, MNRAS, 335, L51

Franceschini, A., Lonsdale, C., & the SWIRE Co-Investigator Team. 2003, in The Mass of Galaxies at Low and High Redshift, ed. R. Bender & A. Renzini (Berlin: Springer), 338

Gautier, T. N., Boulanger, F., Perault, M., & Puget, J. L. 1992, AJ, 103, 1313

Geballe, T. R., et al. 2002, ApJ, 564, 466

Giacconi, R., et al. 2001, ApJ, 551, 624

Gilli, R. 2002, Adv. Space Res., in press (astro-ph/0303115)

Gilli, R., Salvati, M., & Hasinger, G. 2001, A&A, 366, 407

Granato, G. L., Silva, L., Monaco, P., Panuzzo, P., Salucci, P., De Zotti, G., & Danese, L. 2001, MNRAS, 324, 757

Gregg, M. D., Lacy, M., White, R. L., Glikman, E., Helfand, D., Becker, R. H., & Brotherton, M. S. 2002, ApJ, 564, 133

Gruppioni, C., et al. 1999, MNRAS, 305, 297

Guiderdoni, B., Hivon, E., Bouchet, F. R., & Maffei, B. 1998, MNRAS, 295, 877

Haas, M., Müller, S. A. H., Chini, R., Meisenheimer, K., Klaas, U., Lemke, D., Kreysa, E., & Camenzind, M. 2000, A&A, 354, 453

Hasinger, G., Burg, R., Giacconi, R., Schmidt, M., Trumper, J., & Zamorani, G. 1998, A&A, 329, 482

Hasinger, G., et al. 2001, A&A, 365, L45

Hauser, M. G., & Dwek, E. 2001, ARA&A, 39, 249

Helou, G., & Beichman, C. 1990, in From Ground-Based to Space-Borne Sub-mm Astronomy, ed. B. Kaldeich (ESA SP-314; Noordwijk: ESA), 117

Ivezic, Z., et al. 2002, AJ, 124, 2364

Ivison, R. J., et al. 2002, MNRAS, 337, 1

Jannuzi, B. T., Dey, A., Brown, M. J. I., Tiede, G. P., & NDWFS Team. 2002, BAAS, 34, 104.01

Jarrett, T. H., Chester, T., Cutri, R., Schneider, S., & Huchra, J. P. 2003, AJ, 125, 525

Jarrett, T. H., Dickman, R. L., & Herbst, W. 1994, ApJ, 424, 852

John, T. L. 1988, A&A, 193, 189

Kaiser, N. 1984, ApJ, 284, L9

Kajisawa, M., & Yamada T. 2001, PASJ, 53, 833

Kaviani, A., Haehnelt, M., & Kauffmann, G. 2003, MNRAS, 340, 739

Kawara, K., et al. 1998, A&A, 336, L9

Kennicutt, R. J., et al. 2003, PASP, 115, 928

Kenter, A., Murray, S., & Meehan, G. 2002, Am. Phys. Soc. Meeting, 17, 108

Kepner, J., Fan, X., Bahcall, N., Gunn, J., Lupton, R., & Xu, G. 1999, ApJ, 517, 78

Kessler, M. F., et al. 1996, A&A, 315, L27

Klaas, U., et al. 2001, A&A, 379, 823

Kodama, T., Bell, E., & Bower, R. 1999, MNRAS, 302, 152

Koerner, D. W., Ressler, M. E., Werner, M. W., & Backman, D. E. 1998, ApJ, 503, L83

Kuraszkiewicz, J. K., et al. 2003, ApJ, 590, 128

Labbe, I., et al. 2003, AJ, 125, 1107

Lacy, M., Laurent-Muehleisen, S., Ridgway, S., Becker, R., & White, R. L. 2001, ApJ, 551, L17

Lagache, G., Dole, H., & Puget, J.-L. 2003, MNRAS, 338, 555

Lagrange, A.-M., Backman, D., Artymowicz, P. 2000, in Protostars and Planets IV, ed. V. Mannings, A. Boss, & S. Russell (Tucson: Univ. Arizona Press), 639

Lahav, O., Nemiroff, R. J., & Piran T. 1990, ApJ, 350, 119

Lahav, O., et al. 2002, MNRAS, 333, 961

Lari, C., et al. 2001, MNRAS, 325, 1173

Le Fevre, O., et al. 2003, A&A, submitted (astro-ph/0306252)

Leitherer, C., et al. 1999, ApJS, 123, 3

Magorrian, J., et al. 1998, AJ, 115, 2285

Maiolino, R., Salvati, M., Bassani, L., Dadina, M., della Ceca, R., Matt, G., Risaliti, G., & Zamorani, G. 1998, A&A, 338, 781

Maiolino, R., et al. 2000, Adv. Space Res., 25, 809

Manners, J. C., et al. 2003, MNRAS, 343, 293

Martín, E. L., Brandner, W., Jewitt, D. C., Simon, T., Wainscoat, R., Connelley, M., Marley, M., & Gelino, C. 2001, PASP, 113, 529

Menanteau, F., Ellis, R. S., Abraham, R. G., Barger, A. J., & Cowie, L. L. 1999, MNRAS, 309, 208

Mirabel, I. F., et al. 1999, A&A, 341, 667

Mizumoto, Y., et al. 2003, Subaru/*XMM-Newton* Deep Survey (Mauna Kea: NAOJ)

Moorwood, A. F. M. 1999, in The Universe as Seen by *ISO*, ed. P. Cox & M. Kessler (ESA SP-427; Noordwijk: ESA), 825

Norberg, P., et al. 2002, MNRAS, 332, 827

Oliver, S., et al. 1996, MNRAS, 280, 673

———. 2000, MNRAS, 316, 749

Oppenheimer, B. R., Kulkarni, S. R., & Stauffer, J. R. 2000, in Protostars and Planets IV, ed. V. Mannings, A. Boss, & S. Russell (Tucson: Univ. Arizona Press), 639

Papovich, C., & Bell E. F. 2002, ApJ, 579, L1

Pearce, F. R., Jenkins, A., Frenk, C. S., White, S. D. M., Thomas, P. A., Couchman, H. M. P., Peacock, J. A., & Efstathiou, G. 2001, MNRAS, 326, 649

Pérez García, A. M., & Rodríguez Espinosa, J. M. 2001, ApJ, 557, 39

Phillips, J., Weinberg, D. H., Croft, R. A. C., Hernquist, L., Katz, N., & Pettini, M. 2001, ApJ, 560, 15

Pierre, M., Valtchanov, I., & Refregier, A. 2002, in New Visions of the X-Ray Universe in the *XMM-Newton* and *Chandra* Era, ed. F. Jansen (ESA SP-488; Noordwijk, ESA), 26

Pierre, M., et al. 2003, A&A, submitted (astro-ph/0305191)

Poggianti, B. M., Bressan, A., & Franceschini, A. 2001, ApJ, 550, 195

Polletta, M., Courvoisier, T. J.-L., Hooper, E. J. D., & Wilkes, B. J. 2000, A&A, 362, 75

Polletta, M., Lonsdale, C. J., Xu, C. K., & Wilkes, B. J. 2003, ApJ, submitted

Priddey, R., & McMahon, R. 2001, MNRAS, 324, L17

Reid, I. N., et al. 1999, ApJ, 521, 613

Rieke, G., et al. 2003, *SIRTF* Guaranteed Time Observation Program

Rigopoulou, D., Spoon, H., Genzel, R., Lutz, D., Moorwood, A., & Tran, Q. 1999, AJ, 118, 2625

Rodighiero, G., Fadda, D., Alessandra, G., Lari, C., & Franceschini, A. 2003, in Exploiting the ISO Data Archive: Infrared Astronomy in the Internet Age, ed. C. Gry et al. (ESA SP-511; Noordwijk: ESA), in press

Roelfsema, P. R., et al. 1996, A&A, 315, L289

Rosati, P., et al. 2002, ApJ, 566, 667

Rowan-Robinson, M. 2001, ApJ, 549, 745

———. 2003, MNRAS, submitted

Rowan-Robinson, M., et al. 1997, MNRAS, 289, 490

———. 2000, MNRAS, 314, 375

Saunders, W., Frenk, C., Rowan-Robinson, M., Lawrence, A., & Efstathiou, G. 1991, Nature, 349, 32

Saunders, W., et al. 2000, MNRAS, 317, 55

Sawicki, M. 2002, AJ, 124, 3050

Schlegel, D. J., Finkbeiner, D. P., & Davis, M. 1998, ApJ, 500, 525

Schreier, E. J., et al. 2001, ApJ, 560, 127

Scott, S., et al. 2002, MNRAS, 331, 817

Shupe, D. L., Fang, F., Hacking, P. B., & Huchra, J. P. 1998, ApJ, 501, 597

Shupe, D., Huber, A. K., & Hacking, P. 1996, Proc. SPIE, 2817, 1057

Siana, B., Smith, H. E., Lonsdale, C. J., & the SWIRE Team. 2002, BAAS, 34, 1195

Silk, J., & Rees, M. 1998, A&A, 331, L1

Silva, L., Granato, G. L., Bressan, A., & Danese, L. 1998, ApJ, 509, 103

Simcoe, R. A., Metzger, M. R., Small, T. A., & Araya, G. 2000, AAS Meeting, 196, 5209

Simpson, C., & Eisenhardt, P. 1999, PASP, 111, 691

Soifer, B. T., Boehmer, L., Neugebauer, G., & Sanders, D. 1989, AJ, 98, 766

Somerville, R., Lemson, G., Sigad, Y., Dekel, A., Kauffmann, G., & White, S. 2001, MNRAS, 320, 289

Strauss, M. A., & Willick, J. 1995, Phys. Rep., 261, 271

Sturm, E., Lutz, D., Tran, D., Feuchtgruber, H., Genzel, R., Kunze, D., Moorwood, A. F. M., & Thornley, M. D. 2000, A&A, 358, 481

Surace, J. A., Sanders, D. B., & Evans, A. S. 2000, ApJ, 529, 170

Szalay, A. S., Connolly, A. J., & Szokoly, G. P. 1999, AJ, 117, 68

Tran, D. 1998, Ph.D. thesis, Univ. Paris XI

Valtchanov, I., et al. 2003, A&A, submitted (astro-ph/0305192)

Verstraete, L., Puget, J.-L., Falgarone, E., Drapatz, S., Wright, C., & Timmermann, R. 1996, A&A, 315, L337

Williams, R., et al. 1996, AJ, 112, 1335

Willick, J. A., & Strauss, M. A. 1998, ApJ, 507, 64

Xu, C. K., Lonsdale, C. J., Shupe, D. L., Franceschini, A., Martin, D., & Schiminovich, D. 2003, ApJ, 587, 90

Xu, C. K., Lonsdale, C. J., Shupe, D. L., O'Linger, J., & Masci, F. 2001, ApJ, 562, 179

Yang, Y., Mushotsky, R., Barger, A., Cowie, L., Sanders, D., & Steffen, A. 2003, ApJ, 585, L85

York, D. G., et al. 2000, AJ, 120, 1579